NASA TECHNICAL MEMORANDUM

NASA TM X-2295

NASA TM X-2295

FLIGHT INVESTIGATION OF INSTALLATION EFFECTS ON A PLUG NOZZLE INSTALLED ON AN UNDERWING NACELLE

by Nick E. Samanich and Roger Chamberlin

Lewis Research Center
Cleveland, Ohio 44135

NATIONAL AERONAUTICS AND SPACE ADMINISTRATION • WASHINGTON, D. C. • JULY 1971

1. Report No.	2. Government Accession No.	3. Recipient's Catalog No.
NASA TM X-2295		

4. Title and Subtitle	5. Report Date
FLIGHT INVESTIGATION OF INSTALLATION EFFECTS ON A PLUG NOZZLE INSTALLED ON AN UNDERWING NACELLE	July 1971
	6. Performing Organization Code

7. Author(s)	8. Performing Organization Report No.
Nick E. Samanich and Roger Chamberlin	E-5546
	10. Work Unit No. 720-03

9. Performing Organization Name and Address	11. Contract or Grant No.
Lewis Research Center National Aeronautics and Space Administration Cleveland, Ohio 44135	

12. Sponsoring Agency Name and Address	13. Type of Report and Period Covered
National Aeronautics and Space Administration Washington, D.C. 20546	Technical Memorandum
	14. Sponsoring Agency Code

15. Supplementary Notes

16. Abstract

Several variations of plug nozzles were tested using an F-106B aircraft in the Mach range 0.6 to 1.3. These nozzles simulated the subsonic configurations of variable-geometry plug nozzles designed for Mach 2.8 operation. The nozzles were tested with a J85-GE-13 turbojet engine and the data compared to that of 0.34-scale isolated wind tunnel models. For most of the configurations tested, no significant installation effect was measured between Mach 0.8 and 0.9. There was an adverse effect at lower speeds and at Mach numbers from 1.0 to 1.2, and a favorable effect at Mach 0.95. The major differences between the isolated and installed nozzle performance resulted from changes in pressure forces on the plug surface.

17. Key Words (Suggested by Author(s))	18. Distribution Statement
Airframe installation effects Plug nozzle Propulsion system Transonic Flight test	Unclassified - unlimited

19. Security Classif. (of this report)	20. Security Classif. (of this page)	21. No. of Pages	22. Price*
Unclassified	Unclassified	57	$3.00

*For sale by the National Technical Information Service, Springfield, Virginia 22151

FLIGHT INVESTIGATION OF INSTALLATION EFFECTS ON A PLUG NOZZLE INSTALLED ON AN UNDERWING NACELLE

by Nick E. Samanich and Roger Chamberlin

Lewis Research Center

SUMMARY

Several configurations of a plug nozzle were installed on an underwing nacelle mounted on an F-106B aircraft. A J85-GE-13 turbojet engine provided primary flow. Nozzle performance was investigated in the Mach range from 0.6 to 1.3. Installation effects were determined by comparing the performance with 0.34-scale isolated cold-flow results which were obtained with a 21.6-centimeter (8.5-in.) diameter model in the Lewis 8- by 6-Foot Wind Tunnel. The configurations tested simulate subsonic geometries of nozzles designed for high-pressure-ratio operation near Mach 2.8. Parametric changes in plug truncation, shroud extension, corrected secondary weight flow, and nozzle pressure ratio were made. The effect of nacelle shape immediately upstream of the plug assembly was also investigated.

In most cases the installation had little effect on nozzle performance at Mach numbers from 0.8 to 0.9. An adverse effect was measured at lower speeds and at Mach numbers from 1.0 to 1.2, but the installed nozzle performance peaked at Mach 0.95 and was significantly higher than the isolated nozzle data. The favorable effect resulted from an amplification of the pressure rise behind the terminal shock resulting from the combination of the wing and nacelle flow fields. The major difference in performance between isolated and installed configurations resulted from changes in pressure forces on the plug surface. The installation caused appreciable circumferential pressure variations on the plug nozzle assembly immediately aft of the wing trailing edge. The high pressures on top caused the secondary cooling air to exit asymmetrically in some instances. No evidence of unsteady pressure on the plug surface was detected by high-response pressure transducers.

Nozzle performance (thrust-minus-drag ratioed to ideal primary thrust) of approximately 0.95 was measured at Mach 0.90 at an exhaust nozzle pressure ratio of 3.7 and approximately 3-percent corrected secondary flow. Increasing corrected secondary flow raised nozzle performance over the range tested (2 to 9 percent), primarily because of the increase in secondary-flow exit momentum. The configuration having a boattailed nacelle afterbody and smaller plug was less sensitive to changes in nozzle pressure ratio than the cylindrical nacelle with larger plug. The degree of plug truncation which was possible without adversely affecting plug performance appeared to be sensitive to configuration and Mach number.

INTRODUCTION

The Lewis Research Center is conducting an investigation into the effects of airframe installation on the performance of several representative turbojet exhaust nozzles operating in the transonic speed range (refs. 1 to 3). The powerplant installation being studied is a nacelle in an aft underwing location. One of the nozzle types being tested is a plug nozzle. The plug nozzle provides good aerodynamic performance, has a low infrared signature, can operate efficiently over a range of pressure ratios with minimal geometry changes and may be quieter than other nozzle types (refs. 4 and 5).

Original investigations of plug nozzles were made with isentropic external expansion surfaces (refs. 6 to 9). The high lip angles of the primary flap, characteristic of these nozzles, develop low base pressure with accompanying high drag over most of the Mach number range. A study was made of the effect of lip angle on internal performance of conical and contoured plugs (ref. 10). It was shown that on a conical plug, the lip angle could be reduced considerably below the theoretical value required for complete external expansion without incurring any appreciable performance penalty. The shallower lip angles tend to minimize the adverse effect of the external stream. The effect of conic plug angle was explored in a series of British experiments using a 0° lip angle and a translating cylindrical shroud to provide variable internal expansion (refs. 11 and 12). High efficiencies were demonstrated over a wide range of pressure ratios and similar results were shown in reference 13. The British study also showed that decreasing conic plug angle had a favorable effect with a practical optimum at about 10° half-angle. A brief investigation of the effect of plug truncation was also made by the British (ref. 12) and more extensively by Schmeer, Kirkham, and Salters (ref. 14). More recently some studies were made with a 10° half-angle plug nozzle with varying primary throat area simulating both hinged and translating primary flaps (refs. 15 and 16).

A flight test program was initiated to determine installation effects on a large-scale plug nozzle design, free of model blockage and tunnel wall effects which are usually present in a wind tunnel in the transonic region. Flight tests were conducted with an F-106B aircraft modified to carry two 63.5-centimeter (25.0-in.) diameter nacelles, aft mounted under the wing. The nacelles had normal shock inlets and contained J85-GE-13 turbojet engines. The plug nozzle was installed in the left nacelle (fig. 1) and had a 10° half-angle conical plug with a fixed primary throat area ($A^* = 710$ cm^2, or 110 in.^{2}) which permitted operation at part speed and at military power. The afterburner-can of the research engine was modified to provide for attachment of the plug. The tests included several variations of the nozzle design. Parametric changes in plug truncation and shroud extension were made. The effect of nacelle shape immediately upstream of the nozzle assembly was also investigated. The test conditions which were varied

included corrected secondary weight flow, from 2 to 9 percent of primary weight flow; exhaust nozzle pressure ratio, from 2.3 to 5.5; and flight Mach number, from 0.6 to 1.3.

The results include comparisons of the flight nozzle performance with results from 0.34-scale isolated cold-flow tests obtained during an investigation in the Lewis 8- by 6-Foot Supersonic Wind Tunnel reported in reference 17. Static performance of the flight hardware is reported in reference 18. Other results include evaluations of nozzle performance and secondary flow pumping characteristics, and a breakdown of the forces on each of the various nozzle components.

APPARATUS AND PROCEDURE

Installation

Details of the airplane modifications and the nacelle-engine assembly are given in reference 3. A schematic of the research nacelle and plug nozzle is shown in figure 2. The nacelle was located at the 32-percent semispan with a downward incidence of $4\frac{1}{2}^{\circ}$ (relative to the wing chord) so that the aft portion of the nacelle was tangent to the aft wing lower surface. The nacelle had 0° cant and was positioned to provide approximately 0.64-centimeter (0.25-in.) clearance at the wing trailing edge. The apex of the full-length plug was 129.3 centimeters (50.9 in.) aft of the wing trailing edge. Details of the wing modifications, nacelle shape, and mounting strut are given in reference 19. The strut with the wide fairing of reference 19 was used.

The gas generator for the plug nozzle was a J85-GE-13 turbojet engine with afterburner. The variable-area nozzle was removed and replaced with a fixed plug nozzle. The plug nozzle was attached to the afterburner exit using a packing gland slip joint. The plug loads were taken out through three struts. Secondary cooling air was supplied from the inlet and metered at the periphery of the compressor face by a calibrated rotary valve.

Test Hardware

The various plug assemblies tested are shown in figures 3 to 5. The basic plug body (fig. 6) was a 10° half-angle conic structure which was attached to the nacelle by three equally spaced hollow support struts. A nickel-chromium-base alloy (Rolled Alloy 333) was used predominantly in the test hardware. A weight breakdown of the basic assembly is presented in table I. The same plug body was used in all the assemblies. The basic plug size (fig. 6) was determined by several factors. It was desired to have

the largest plug possible consistent with the nacelle diameter of 63.5 centimeters (25.0 in.), a secondary flow area large enough to permit approximately 12-percent coolant flow, and a primary throat area permitting military operation of the J85-GE-13 engine (710 cm^2 or 110 $in.^2$). A restriction to military or part-power operation was imposed to limit the plug design temperature to 1006 K (1810° R), thereby eliminating any nozzle cooling requirements. The 17° half-angle conical primary flap was designed to represent a hinged-iris-type nozzle operating at its minimum area with a capability of 60-percent area modulation. Secondary cooling air was discharged over the primary nozzle flap through an annular passage with a minimum flow area of approximately 297 square centimeters (46 $in.^2$).

The maximum efficiency of this type of plug nozzle depends to a large degree on the pressure force on the external surface of the primary flap. At low-to-moderate nozzle pressure ratios, with the shroud retracted, the pressures on the flap are not influenced by the primary jet but are dependent solely on the secondary and external flow over it. At high pressure ratios, the shroud is extended and its position affects the expansion characteristics of the primary and secondary streams and is therefore critical. Shroud positions having the trailing edge ahead of or near the primary flap shoulder appear to be near optimum for low-pressure-ratio operation. Two shroud lengths were tested with the cylindrical nacelle configuration, both designed for low-pressure-ratio operation: one was positioned such that its trailing edge was in the same plane as the primary flap shoulder ($x/l = -0.08$) and the other slightly upstream ($x/l = -0.12$).

Sections of the plug were removable to provide truncation at approximately 75 and 50 percent of its full length. Base caps were available for closing the truncated plugs. With the base caps removed (open base), approximately 1 to 2 percent of the secondary air was estimated to flow into the cavity.

The basic configuration tested had a shroud whose ratio of exit area to primary throat area A_e/A^* was 4.60, corresponding to a pressure ratio of 37.0 at a specific-heat ratio of 1.34. (All symbols are defined in appendix C.) In order to examine the effect of the installation on a lower pressure ratio design (27.0), the primary flap was lengthened and the throat was moved 30.5 centimeters (12.0 in.) downstream, maintaining the same throat area, as shown in the lower part of the bottom sketch in figure 6. (The basic cylindrical nacelle had the primary exit plane approximately 6.4 cm (2.5 in.) behind the wing trailing edge.) The shroud internal exit diameter was then reduced to 57.18 centimeters (22.51 in.) by means of a rounded boattail on the nacelle. This provided a ratio of shroud exit area to primary throat area A_e/A^* of 3.75, corresponding to a pressure ratio of 27.0 at a specific-heat ratio of 1.34. The exit of the new primary flap was located at the largest plug diameter compatible with the smaller shroud diameter and simulating a hinged iris primary operating at its minimum area with the capability of 60-percent area modulation. The secondary exit flow area was approximately

316 square centimeters (49 $in.^2$). Coordinates of the nacelle boattail and primary flap are given in figures 7 and 8. Three shroud extensions were tested with the boattailed nacelle and 100-percent plug. They were a retracted shroud suitable for low-pressure-ratio operation whose exit was located in the same plane as the primary flap "simulated" hinge ($x'/\ell' = -0.171$) and two extensions corresponding to positions which might be suitable for, or unavoidably encountered during, a typical flight acceleration profile. The extended shrouds tested terminated in the primary exit plane ($x'/\ell' = 0.005$) and 16.37 centimeters (6.44 in.) downstream of the primary exit ($x'/\ell' = 0.177$). A shroud extending approximately 36.09 centimeters (14.21 in.) downstream of the primary exit would be required for optimum performance when operating near the nozzle design pressure ratio of 27.0. The fully retracted shroud was also tested with the plug truncated to approximately 65 percent of full length. The truncated plug was tested with and without a base cap.

The effect of a tapered nacelle geometry on plug nozzle performance was also investigated. The tapered outer fairing, shown in the upper portion of figure 6, simulated the juncture of two conic sections with a maximum diameter of 69.1 centimeters (27.2 in.). Except for the external geometric difference, the configuration was identical to the cylindrical nacelle assembly with retracted shroud ($x/\ell = -0.08$). The top of the tapered nacelle was cut flat to maintain an approximate 0.64-centimeter (0.25-in.) clearance with the fixed portion of the wing elevon (fig. 9(b)).

Instrumentation

A new data recording system was developed specifically for the F-106 program, and as a result it was possible to instrument the plug nozzle quite extensively, see figure 9. The plug body had six area-weighted rows of 15 static-pressure orifices in each row, spanning the length of the plug as shown. The plug configurations truncated to 50 and 75 percent of full length had nine and five static-pressure orifices in the base caps, respectively. Three internal cavity pressures were used with the open-base configurations. A row of 11 thermocouples with the junctures imbedded in the skin were located at a meridian angle of 45° on the plug body. The primary flaps, aft nacelle skin, and shroud extensions had four rows of static-pressure orifices equally spaced around the circumference. Internal static pressures were measured on the boattailed nacelle extended shrouds as well as skin temperatures on the longest shroud, $x'/\ell' = 0.177$, at meridian angles of 120° and 180°. Static pressures on both the forward and rearward facing surfaces of the double conic section of the tapered nacelle were measured at meridian angles of 45°, 90°, 135°, and 180°. Four total-pressure and total-temperature probes were mounted near the secondary exit to monitor the secondary-flow conditions. On the

boattailed and tapered nacelle configurations, a 10.2-centimeter (4.0-in.), six-tube, total-pressure, boundary-layer rake was mounted on the bottom of the nacelle at station 524.5 centimeters (206.5 in.)(fig. 9).

As shown in figure 2, the nacelles were supported by two attachment links with a strain-gage, load-cell assembly located between the links. The front and rear links were each attached to the wing and nacelle with fittings having low friction bearings. Each link was installed so that a line through the axis of rotation of the upper and lower bearings was perpendicular to the nacelle thrust axis. This system of links transfers only the loads parallel to the nacelle axis to the load cell. Accelerometers in the nacelle provide corrections for axial weight components and acceleration effects.

Procedure

All flights were made out of Cleveland Hopkins Airport with two 185.3-kilometer (100-n-mi) test corridors over Lake Erie used during data acquisition. To utilize the maximum potential of the fuel available, data were taken at both subsonic and supersonic Mach numbers for most flights. A total of 16 flights were made for the plug nozzle test series. A prescribed flight trajectory was followed which resulted in a repeatable angle-of-attack and elevon-deflection schedule (see figs. 10 and 11).

For each configuration the engine was run at 100-percent mechanical speed, the corrected secondary-weight-flow ratio was set at about 0.03, and data were acquired over a range of Mach numbers from 0.6 to 1.3. With some of the assemblies, secondary flow and exhaust nozzle pressure ratio were varied by modulating the secondary-weight-flow valve and J85 engine speed, respectively. The exact pressure ratio and secondary weight flow for all configurations tested at military power are given in appendix A.

Data Reduction

Engine airflow was determined using prior engine calibration data (ref. 20) along with in-flight measurements of engine speed, pressure, and temperature at the compressor face. Knowing compressor inlet flow, the total pressure and temperature at the turbine discharge, and the fuel flow rates, other parameters at the primary nozzle exit, such as effective area A_8, total pressure P_8, and total temperature T_8, were obtained from previous calibrations. Calibrations of the secondary-flow-valve pressure drop and position were used to determine secondary airflow.

Prior in-flight thrust system calibrations were made with reference cylindrical ejectors on both nacelles. The ejector thrust characteristics in conjunction with the

load-cell readings were used to determine a nacelle tare force. The tare force, consisting of the inlet momentum and all external forces on the nacelle forward of the nozzle attachment flange (nacelle station 457.2 cm (180 in.)), was shown to be a function of flight speed and inlet spillage. Knowing these two parameters during the research flights enabled the tare to be determined. The load-cell measurement was used in combination with the tare force to determine nozzle gross thrust minus drag. Details of the calibrations and of the thrust-measuring system for the F-106 are presented in reference 21.

The basic nozzle performance parameter selected was a ratio of measured gross thrust-minus-drag to the ideal thrust of the primary flow. The ideal thrust of the primary was calculated from the known mass-flow rate expanded isentropically to ambient pressure p_0. Pressures were integrated along the various surfaces and the calculated axial forces are presented in terms of percent of ideal primary thrust. Individual pressure distributions are also shown for the various components.

RESULTS AND DISCUSSION

Isolated (Wind Tunnel) and Installed (Flight) Comparisons

Isolated models of the flight hardware were tested on a 21.59-centimeter (8.5-in.) diameter (0.34-scale), strut-supported, closed-nose body of revolution in the 8- by 6-Foot Supersonic Wind Tunnel (ref. 17). The cold-flow models were tested over a range of conditions which encompassed or were near the F-106 operating schedule. Previous wind tunnel tests indicated that the tunnel data in the Mach-1.0-to-1.3 range may not be representative of true isolated data since tunnel interference appeared to cause higher pressures on the external nozzle surfaces (ref. 22).

Performance Comparisons

Performance of most of the configurations which were flight tested is compared with 0.34-scale, isolated, cold-flow model performance in figure 12. The performance of the isolated nozzles declined gradually as Mach number was increased, with a rather sharp decrease occurring between Mach 0.9 and 1.0. The installed nozzles, on the other hand, exhibited an increase in thrust coefficient with increasing Mach number which peaked at Mach 0.95 and then sharply declined, reaching a minimum near Mach 1.0. For most of the configurations tested, no significant installation effect was observed between Mach 0.8 and 0.9. There were adverse effects at lower speeds and at Mach numbers from 1.0 to 1.2, and a favorable effect at Mach 0.95. This favorable

effect is a result of a terminal shock which moves back over the nacelle, and at a Mach number of 0.95 is just upstream of the nozzle assembly. As described in reference 2, the combination of the flow field of the wing and the flow field around the nacelle, which is reflected by the lower surface of the wing, amplifies the recompression of the flow through the shock and over the nozzle assembly. These higher pressures reduce the nozzle drag, increasing the nozzle performance. As Mach number was increased beyond 0.95, a sharp drop in efficiency was measured which was considerably greater than measured in the isolated tests. The drop in performance can be attributed to the low static pressures resulting when the terminal shock moves off the nozzle at Mach 0.96 to 1.0. There is indication that the terminal shock on the isolated nozzles tested in the wind tunnel did not move off the nozzle until a Mach number somewhat greater than 1.1.

Component Force Comparisons

The plug body and primary flap forces calculated by a pressure integration are presented in figure 13 for both the isolated and installed tests. For the installed nozzle the primary flap and plug pressure forces both reflect the same general trend as the performance. In general, it can be seen that the component most affected by the installation appears to be the plug body. The sharp drop in pressure force on the plug surface associated with terminal shock movement can be seen between Mach 0.96 and 1.0 in the flight tests but appears to be somewhat delayed to higher speeds in the wind tunnel.

A comparison of the circumferential pressure distributions on the retracted shrouds of the cylindrical and boattailed nacelles is made in figures 14 and 15. In all cases the flow off the top of the wing washes down on the nozzle assembly and causes higher pressures in the upper quadrant immediately aft of the wing trailing edge. At Mach 0.80 (figs. 14(a) and 15(a)), the recompression on the installed nozzle is not much stronger than that of the isolated nozzle, as can be seen by the comparative pressure levels. As the terminal shock moves back closer to the nozzle at Mach 0.90 (figs. 14(b) and 15(b)), higher pressures are measured on the installed assembly. At low supersonic speeds such as Mach 1.1, the terminal shock is off the installed nozzle. However, in the isolated case, the higher pressures on the primary flap (figs. 14(c) and 15(c)) may indicate the terminal shock is still in the vicinity of the nozzle. Pressure distributions on the plug surface are presented in appendix B.

Figure 16 presents the pressure distribution on the nacelle boattail and primary flap for the boattailed nacelle with the intermediate shroud extension. For this configuration the primary flap is completely shielded and the circumferential pressure asymmetry is only present on the boattail. The pressure distributions on the external surfaces of the fully extended shroud (not presented) were very similar to those of the intermediate extension.

The cylindrical shroud extension caused the external flow to turn axially at the boattail-shroud juncture. This flow compression fed forward onto the boattail and resulted in lower boattail drags (figs. 15 and 16). The external primary flap pressures reflected the overexpanded corrected secondary weight flow with corresponding low pressures. Figure 17 presents the pressure distribution on the tapered fairing and primary flap for the tapered nacelle configuration. Less circumferential pressure variation is evidenced on the primary flap, as well as a higher overall pressure level than was measured with the cylindrical nacelle (fig. 14). Only small differences in primary flap pressures were measured compared to isolated results.

Pumping Characteristics

The effect of the installation on the pumping characteristics of the three basic configurations tested at Mach 0.90 and a nominal corrected secondary-weight-flow ratio of 0.03 is presented in figure 18. At this Mach number the secondary total pressure was lower than ambient p_0 for the cylindrical and tapered nacelle assemblies. The lower secondary pressure did result in a secondary exit momentum which could be interpreted as a drag force.

Since the secondary pumping of this type of plug nozzle (with the shroud retracted) is achieved primarily by the external stream rather than by the primary jet, it would be expected to be relatively sensitive to distortion of the external flow field. At Mach 0.90 the cylindrical nacelle assembly appeared to be most affected by the installation requiring approximately 9 percent higher secondary pressure to pump the same secondary flow when installed (fig. 18(a)). The boattailed nacelle, which had a relocated throat and secondary exit downstream of the wing trailing edge, required only 2 percent higher secondary pressure when installed to pump the same weight flow (fig. 18(b)). The tapered nacelle (fig. 18(c)) showed no measurable difference in pumping characteristics due to installation.

Installed Nozzle Characteristics (Flight)

Several variations of a plug nozzle installed on an underwing nacelle were tested at Mach numbers from 0.6 to 1.3. Although the nacelle location was fixed relative to the aircraft wing (fig. 2), the specific location of the nozzle components for the various assemblies was somewhat different. These installation differences (see APPARATUS AND PROCEDURE section) should be kept in mind when comparisons of the flight-tested nozzles are made.

Effect of Nacelle Geometry

Three different types of nacelle shapes immediately ahead of the nozzles were tested: cylindrical, boattailed, and tapered (see fig. 6). Two retracted shroud extensions were tested with the cylindrical nacelle and their performance is shown in figure 19. The performance of both shrouds followed the same general trend. Performance increased with increasing Mach number, peaked at Mach 0.95, and then dropped sharply near Mach 1.0 as the terminal shock passed over the nozzle. The shortest shroud ($x/l = -0.12$) appeared to perform slightly better over the Mach number range tested. The higher performance is the result of lower primary flap drag. However, in static tests of the same hardware (ref. 18) it was found that the longer shroud extension ($x/l = -0.08$) gave slightly higher performance.

The performance of the three different boattailed-nacelle shroud extensions is shown in figure 20. The highest performance was measured with the retracted shroud and decreased with shroud extension. The drop in performance with the longer extensions resulted from larger areas of overexpansion on the plug and the primary flap surface. Wind tunnel tests on a similar isolated plug nozzle have shown that the benefits of shroud extension at even higher nozzle pressure ratios are not realized below Mach numbers of 1.2 (ref. 15).

A comparison of the performance of the boattailed assembly with retracted shroud ($x'/l' = -0.171$) and the cylindrical nacelle assembly with retracted shroud ($x/l = -0.12$) shows slightly higher performance for the boattailed assembly over the entire Mach number range tested (figs. 19 and 20). In general, the drag on the boattail is offset by higher pressure forces on the plug body and primary flap along with a larger secondary-flow exit momentum.

The tapered nacelle was tested to see the effects on plug performance of an oversized nacelle having a double-conic juncture at its maximum diameter. The assembly was made by using the basic cylindrical nacelle ($x/l = -0.080$) with a tapered fairing externally attached to it. The effect of changing nacelle geometry from the cylindrical to the double-conic shape is shown in figure 21. The presence of the tapered fairing resulted in a flow field that gave a higher nozzle gross thrust coefficient over the Mach number range tested. If the nozzle is charged for the drag on the aft conic surface of the tapered nacelle, performance was still slightly higher than the cylindrical nacelle subsonically, but was slightly lower above Mach 1.0.

Effect of Plug Truncation

The plug body was designed such that two truncations could be tested. For each truncation, base caps were available for closing the base if desired. The base caps did add some length compared to the corresponding open base. The same truncations resulted in different percentage changes for the cylindrical and boattail assemblies because of their corresponding different plug lengths (throat plane to apex). Tests were run with nominal plug lengths of 100, 75, and 50 percent with the $x/l = -0.12$ cylindrical nacelle assembly and with plug lengths of 100 and 65 percent with the $x'/l' = -0.171$ boattailed nacelle.

The thrust characteristics, plug forces, base pressures, and base forces are shown for each truncation in figures 22 and 23. An approximate linear decrease in performance with plug truncation was measured for the configurations with the cylindrical shroud, as shown in figure 22(a). At Mach 0.9 a 2-percent drop with 50-percent truncation was due primarily to a smaller plug pressure force (fig. 22(b)). (Pressure distributions on the plug surface are presented in appendix B.) As the terminal shock passed over the plug, between Mach 0.96 and 1.0, the plug base pressures dropped considerably (see fig. 22(d)). The configurations with the nominal 50-percent plug lengths have large base areas compared with the shorter truncation, and therefore a drop in base pressure, as evidenced at supersonic speeds, results in a more significant drag force.

The boattailed nacelle assembly did not show any noticeable loss in performance when the plug was truncated to 67 percent of full length (fig. 23). The change in plug force was small and was generally less than that of the same physical truncation (75 percent) with the cylindrical nacelle. No significant base drag was measured, due primarily to the relatively small base area.

After examining plug truncation effects for the cylindrical and boattailed nacelle assemblies, it can be concluded that the amount of truncation possible, without adversely affecting nozzle performance, is sensitive to configuration and Mach number.

Effect of Secondary Weight Flow

The effect of secondary weight flow on the performance of the cylindrical and boattailed nacelle assemblies is shown in figure 24. The trend of increasing gross thrust coefficient with increasing secondary flow existed over the Mach number range. The full ram drag penalty of the secondary flow is sometimes assessed to the nozzle. This performance parameter, $\left[(F - D) - m_s V_0\right]/F_{i,p}$, also exhibits an increasing trend with increasing secondary weight flow at the subsonic Mach numbers (fig. 25). Although all the component nozzle forces (fig. 26) increase slightly with increasing secondary flow,

the largest increase results from secondary momentum. The increase in the absolute secondary weight flow accounts for 60 to 70 percent of the total performance increase. The agreement in nozzle efficiency obtained from the load cell and that calculated by summation of the component forces is shown in the upper part of the figure. The load-cell system gave an efficiency somewhat lower than calculated for both configurations at Mach 0.9.

Effect of Exhaust Nozzle Pressure Ratio

Nozzle pressure ratio was varied by modulating engine speed for the cylindrical and boattailed nacelle assemblies. Its effect on nozzle thrust coefficient at several Mach numbers is presented in figure 27. At a nominal Mach 0.9 aircraft speed, the performance of the boattailed nacelle with fully retracted shroud was considerably less sensitive to pressure ratio change than the corresponding cylindrical nacelle configuration; reducing pressure ratio from 3.7 to 2.8 resulted in drops in thrust coefficient from 0.94 to 0.90 and from 0.93 to 0.85, respectively.

Pumping Characteristics

Pumping characteristics of the various configurations tested with the full-length plug are shown in figure 28. At Mach 0.90 the cylindrical nacelle assembly required approximately 9 percent lower secondary pressure to pump a comparable secondary flow than the boattailed nacelle assembly with retracted shroud, as seen by comparing figures 28(a) and (c). As the shroud was extended, the pumping characteristics changed, with the longest shroud ($x'/l' = 0.177$ (fig. 28(e)) requiring 18 percent lower secondary pressure to pump the same secondary flow as the shortest shroud extension ($x'/l' = -0.171$). The tapered nacelle required slightly higher pressures to pump secondary flow than the cylindrical nacelle with the same shroud extension ($x/l = -0.08$).

Component Forces

A breakdown of nozzle component forces over the Mach number range is given in figure 29. The effect of the terminal shock passing over the nozzle between Mach 0.96 and 1.0 produces the largest effect on the plug and primary flap. On the boattailed and tapered nacelle assemblies the effect is also seen on the boattail and tapered fairing (figs. 29(c) to (f)). Figures 29(c) to (e) show the effects of shroud extension with the

boattailed nacelle on the individual components. For the extended shrouds the flow over the boattail is turned axially at the point where the shroud extension begins. This results in a compression which feeds up onto the boattail, with corresponding lower drags. However, much larger internal losses are measured on the plug and primary flap. Figure 29(f) presents the component forces of the nozzle with the tapered nacelle assembly. The favorable effects at subsonic speeds can be seen, as several components show benefits with the tapered nacelle compared with the cylindrical nacelle for comparable shroud extensions (figs. 29 (b) and (f)). Figure 30 compares the performance measured by the load cell and the performance obtained by summing the component forces. There is relatively close agreement between the measured and calculated performance.

Secondary-Flow Profiles

Early in the test series, significant temperature profiles coupled with pressure data indicated some degree of reverse or recirculating flow in regions of the secondary passage near the exit plane. This was apparent only for the cylindrical nacelle assembly, whose secondary exit plane was just upstream of the wing trailing edge. The best indication of the localized recirculation appeared to be gas temperature measurements in the secondary exit plane (fig. 31). When reverse flow did exist, the local secondary gas temperatures were low as a result of the recirculation of the cold ambient air in those regions. It can be seen that at low secondary weight flows the secondary flow had difficulty exiting between the top and inboard 45° sectors, as evidenced by the cool secondary temperature in those regions. Uniform secondary flow was not evidenced until a corrected secondary weight flow of about 0.04 was attained; the average exit secondary Mach number was approximately 0.26 at these conditions.

Temperature Distributions

Temperature distributions along the plug and shroud for the cylindrical and boattailed assemblies are shown in figure 32. The uncooled plug body was essentially uniform in temperature along the entire length, although a slight change in level was measured at the throat of the nozzles. The plug-body skin temperatures downstream of the throat were approximately 93 and 96 percent of the combustion gas temperature T_8 for the cylindrical and boattailed nacelle assemblies, respectively.

The most extended shroud tested with the boattailed nacelle had two rows of thermocouples located on the internal surface of the shroud both in line with (120°) and in between (180°) two plug support struts. The 180° row indicated slightly cooler skin

temperatures, with the trend of increasing temperature with distance aft indicated on both rows. The general temperature level measured on the shroud skin was approximately 40 percent of the main combustion total temperature T_8.

Boundary Layer

A boundary-layer survey was made with a 10.16-centimeter (4.0-in.) rake on the bottom of the nacelle for the boattailed and tapered assemblies. On the boattailed nacelle the rake was located just ahead of the boattail (nacelle station 524.5 cm, or 206.5 in.) as can be seen in figure 4(a). With the tapered nacelle (see fig. 5(b)), the rake was located perpendicular to the aft surface of the tapered fairing just ahead of the trailing edge (nacelle station 523.2 cm, or 206.0 in.).

The velocity profile for the boattailed nacelle assembly at various Mach numbers with the engine at military power and a corrected secondary flow of about 0.03 is shown in figure 33(a). The velocity profile is defined as the ratio of the local velocity to the velocity at a distance 10.16 centimeters (4.0 in.) from the surface. The measurements indicate a boundary layer considerably thicker than that estimated by using flat-plate theory. The boundary layer measured with the tapered nacelle is shown in figure 33(b). The data indicate a localized separation or vortex shedding in the boundary layer near the shroud trailing edge, apparently a result of the double-cone shoulder. The effect of inlet spillage on boundary-layer profile is shown in figure 34 at Mach 0.9. Comparison is made with a 1/7-power profile assuming a turbulent 10.16-centimeter (4.0-in.) thick boundary layer. Increasing inlet spillage appears to generate a profile approaching the 1/7 power.

Dynamic Pressure Measurements

Three high-response pressure transducers were used to measure dynamic pressures on the plug surface at 0° and 180° circumferential location about halfway down the full-length plug and in the base cap of the 50-percent truncated plug. The outputs were recorded on an analog tape recorder during each 11.6-second data scan. No evidence of unsteady pressure was detected.

SUMMARY OF RESULTS

Several variations of plug nozzle designs were tested installed under the wing of an F-106B aircraft at Mach numbers from 0.6 to 1.3. The configurations simulated subsonic geometries of nozzles designed for high supersonic speeds (~Mach 2.8). Performance is compared with 0.34-scale, isolated, cold-flow results. The tunnel data between Mach 1.0 and 1.3 may not be representative of true isolated data since tunnel interference appears to cause higher external nozzle pressures. The following results were obtained:

1. In most cases, the installation had little effect on performance at Mach numbers from 0.80 to 0.90. An adverse effect was measured at lower speeds and at Mach numbers from 1.0 to 1.2, but a significant improvement was measured at Mach 0.95.

2. The major differences in performance between isolated and installed assemblies appear to stem from changes in pressure forces on the plug body.

3. The installation caused appreciable circumferential pressure variations on the plug nozzle assembly (high pressures on top) immediately aft of the wing trailing edge and in some instances caused the secondary cooling flow to exit asymmetrically. No evidence of unsteady pressure on the plug surface was detected with high-response pressure transducers.

4. Nozzle gross thrust-minus-drag ratioed to ideal primary thrust of 0.95 was measured at Mach 0.90, at an exhaust nozzle pressure ratio of 3.7 and approximately 3-percent corrected secondary flow.

5. Over the range tested, increasing secondary flow increased nozzle performance primarily because of the secondary flow momentum increase.

6. The performance of the configuration having the boattailed nacelle afterbody and smaller plug was less sensitive to nozzle pressure ratio than the cylindrical nacelle and larger plug.

7. A comparison of the effects of plug truncation with the cylindrical and boattailed nacelle assemblies indicated that the degree of truncation possible without adversely affecting performance is sensitive to configuration and Mach number.

8. Reducing the shroud exit diameter by means of boattailing ahead of the shroud appeared to improve performance over the Mach range tested.

Lewis Research Center,
National Aeronautics and Space Administration,
Cleveland, Ohio, March 8, 1971,
720-03.

APPENDIX A

PRIMARY AND SECONDARY PRESSURE CONDITIONS

Nozzle pressure ratio, corrected secondary weight flow, and secondary pressure ratio are presented over the Mach number range for all configurations tested at nominal military power in figure 35. All configurations show a sharp change in pumping characteristics between Mach 0.96 and 0.98. This is presumably caused by the passage of the terminal shock over the nozzle resulting in lower back pressures at the unchoked secondary exit.

APPENDIX B

PLUG PRESSURE DISTRIBUTIONS

The pressure distributions on the plug surface for the cylindrical nacelle (x/ℓ = -0.12) and boattailed nacelle (x'/ℓ' = -0.171) are shown in figures 36 and 37. There is a marked circumferential asymmetry in the plug pressures with the cylindrical shroud. The pressures near the top, or 0° line, are affected by the flow washing down off the wing trailing edge. The expansion characteristics on conical plug surfaces have been studied in previous tests (ref. 23). A free boundary develops between the nozzle exhaust and the external flow. This free boundary is changed locally by the flow off the wing. The result is a phase shift in the pressure oscillations in this area. The out-of-phase relation between the pressures on the top and bottom of the plug surface is most noticeable at flight Mach numbers M_0 of 0.85 (fig. 36(b)), 0.88 (fig. 36(c)), and 0.95 (fig. 36(d)), where they are almost 180° out of phase over most of the plug surface. At M_0 = 1.2 (fig. 36(e)) the terminal shock has passed over the nozzle and off the plug, and the wing flow has a lessened effect on the nozzle pressures.

The circumferential pressure distribution along the plug is more uniform for the boattailed nacelle (fig. 37). The flow off the wing has a lesser effect because the relocated primary exit plane with this assembly is further aft of the wing trailing edge.

APPENDIX C

SYMBOLS

A_e	shroud exit area: cylindrical and tapered nacelles, 3167.12 cm^2 (490.87 $in.^2$); boattail nacelle, 1546.47 cm^2 (239.70 $in.^2$)
A^*	nozzle geometric throat area (cold), 710.0 cm^2 (110.0 $in.^2$)
A_8	nozzle effective throat area (hot), cm^2 ($in.^2$)
C_p	pressure coefficient, $(p - p_0)/q_0$
D	drag, N(lb)
d	diameter, cm (in.)
d_n	reference nacelle diameter, 63.5 cm (25.0 in.)
F	nozzle gross thrust, N(lb)
$\frac{F - D}{F_{i,p}}$	nozzle gross thrust coefficient
h	altitude, m (ft)
ℓ	plug length measured from estimated primary throat of cylindrical and tapered nacelle assemblies, nacelle station 535.1 cm (210.67 in.)
ℓ'	plug length measured from estimated primary throat of boattailed nacelle assemblies, nacelle station 565.7 cm (222.71 in.)
M	Mach number
m	inlet capture mass flow, kg/sec (lb/sec)
m_o	ideal mass flow based on 37.37-cm (14.715-in.) diameter inlet, kg/sec (lb/sec)
P	total pressure, N/m^2abs (psia)
p	static pressure, N/m^2abs (psia)
q_o	dynamic pressure, N/m^2abs (psia)
r	radius, cm (in.)
T	total temperature, K (^oR)
V	velocity, m/sec (ft/sec)
x	axial distance measured from estimated primary throat of cylindrical and tapered nacelle assemblies, nacelle station 535.1 cm (210.67 in.)

x'	axial distance measured from estimated primary throat of boattailed nacelle assemblies, nacelle station 565.7 cm (222.71 in.)
y	distance measured along rake perpendicular to shroud surface, cm (in.)
α	angle of attack, deg
β	elevon deflection, deg
δ	boundary layer thickness, cm (in.)
ω	ratio of secondary to primary weight flows
$\omega\sqrt{\tau}$	corrected secondary weight flow
τ	ratio of secondary to primary total temperatures

Subscripts:

b	plug base
c	nozzle component
i	ideal
l	local
p	primary air
pl	plug
s	secondary air
w	plug wall
0	free stream
2	compressor inlet station
8	primary nozzle throat station

REFERENCES

1. Blaha, Bernard J.: Effect of Underwing Engine Nacelle Shape and Location on Boattail Drag and Wing Pressures at Mach Numbers from 0.56 to 1.46. NASA TM X-1979, 1970.

2. Wilcox, Fred A.; Samanich, Nick E.; and Blaha, Bernard J.: Flight and Wind Tunnel Investigation of Installation Effects on Supersonic Cruise-Exhaust Nozzles at Transonic Speeds. Paper 69-427, AIAA, June 1969.

3. Crabs, Clifford C.; Mikkelson, Daniel C.; Boyer, Earle O.: An Inflight Investigation of Airframe Effects on Propulsion System Performance at Transonic Speeds. Presented at the 13th Annual Symposium of the Society of Experimental Test Pilots, Los Angeles, Calif., Sept. 25-27, 1969.

4. Darchuk, George V.; and Balombin, Joseph R.: Noise Evaluation of Four Exhaust Nozzles for Afterburning Turbojet Engine. NASA TM X-2014, 1970.

5. Martlew, D. L.: Noise Associated With Shock Waves in Supersonic Jets. Aircraft Engine Noise and Sonic Boom. Conf. Proc. No. 42, AGARD, May 1969.

6. Krull, H. George; and Beale, William T.: Comparison of Two Methods of Modulating the Throat Area of Convergent Plug Nozzles. NACA RM E54L08, 1955.

7. Krull, H. George; and Beale, William T.: Effect of Outer-Shell Design on Performance Characteristics of Convergent-Plug Exhaust Nozzles. NACA RM E54K22, 1955.

8. Krull, H. George; and Beale, William T.: Effect of Plug Design on Performance Characteristics of Convergent-Plug Exhaust Nozzles. NACA RM E54H05, 1954.

9. Ciepluch, Carl C.; Krull, H. George; and Steffen, Fred W.: Preliminary Investigation of Performance of Variable-Throat Extended-Plug-Type Nozzles Over Wide Range of Nozzle Pressure Ratios. NACA RM E53J28, 1954.

10. Krull, H. George; Beale, William T.; and Schmiedlin, Ralph F.: Effect of Several Design Variables on Internal Performance of Convergent-Plug Exhaust Nozzles. NACA RM E56G20, 1956.

11. Herd, R. J.; Golesworthy, G. T.; and Herbert, M. V.: The Performance of a Centrebody Propelling Nozzle with a Parallel Shroud in External Flow, Part I. Rep. ARC-CP-841, Aeronautical Research Council, Gt. Britain, 1966.

12. Herbert, M. V.; Golesworthy, G. T.; and Herd, R. J.: The Performance of a Centrebody Propelling Nozzle with a Parallel Shroud in External Flow, Part II. Rep. ARC-CP-894, Aeronautical Research Council, 1966.

13. Bresnahan, Donald L.; and Johns, Albert L.: Cold Flow Investigation of a Low Angle Turbojet Plug Nozzle with Fixed Throat and Translating Shroud at Mach Numbers From 0 to 2.0. NASA TM X-1619, 1968.

14. Schmeer, James W.; Kirkham, Frank S.; and Salters, Leland B., Jr.: Performance Characteristics of a 10^{o} Conical Plug Nozzle at Mach Numbers up to 1.29. NASA TM X-913, 1964.

15. Bresnahan, Donald L.: Experimental Investigation of a 10^{o} Conical Turbojet Plug Nozzle with Iris Primary and Translating Shroud at Mach Numbers from 0 to 2.0. NASA TM X-1709, 1968.

16. Bresnahan, Donald L.: Experimental Investigation of a 10^{o} Conical Turbojet Plug Nozzle with Translating Primary and Secondary Shrouds at Mach Numbers from 0 to 2.0. NASA TM X-1777, 1969.

17. Harrington, Douglas E.: Performance of a 10^{o} Conical Plug Nozzle with Various Primary Flap and Nacelle Configurations at Mach Numbers from 0 to 1.97. NASA TM X-2086, 1970.

18. Huntley, Sidney C.; and Samanich, Nick E.: Peformance of a 10^{o} Conical Plug Nozzle Using a Turbojet Gas Generator. NASA TM X-52570, 1969.

19. Mikkelson, Daniel C.; and Head, Verlon L.: Flight Investigation of Airframe Installation Effects on a Variable Flap Ejector Nozzle of an Underwing Engine Nacelle at Mach Numbers from 0.5 to 1.3. NASA TM X-2010, 1970.

20. Antl, Robert J.; and Burley, Richard R.: Steady-State Airflow and Afterburning Performance Characteristics of Four J85-GE-13 Turbojet Engines. NASA TM X-1742, 1969.

21. Groth, Harold W.: Nozzle Performance Measurement on Underwing Nacelles on an F-106 Utilizing Calibrated Engines and Load Cells. Presented at AIAA Seventh Propulsion Joint Specialist Conference, Salt Lake City, Utah, June 14-18, 1971.

22. Blaha, Bernard J.; and Bresnahan, Donald L.: Wind Tunnel Installation Effects on Isolated Afterbodies at Mach Numbers from 0.56 to 1.5. NASA TM X-52581, 1969.

23. Wasko, Robert A.; and Harrington, Douglas E.: Performance of a Collapsible Plug Nozzle Having Either Two-Position Cylindrical or Variable Angle Floating Shrouds at Mach Numbers from 0 to 2.0. NASA TM X-1657, 1968.

TABLE I. - WEIGHT BREAKDOWN OF

CYLINDRICAL SHROUD ASSEMBLY

[Net center of gravity, station 509.8 cm (200.7 in.).]

Item	Weight	
	kg	lb
Plug	23.0	50.7
Struts and support rings	10.6	23.3
Primary nozzle assembly	18.8	41.5
Outer shroud	24.5	54.1
Shroud attach ring	17.3	38.1
Straps	2.0	4.3
Seal	4.9	10.8
Bolts and fasteners	6.8	15.0
	107.9	237.8

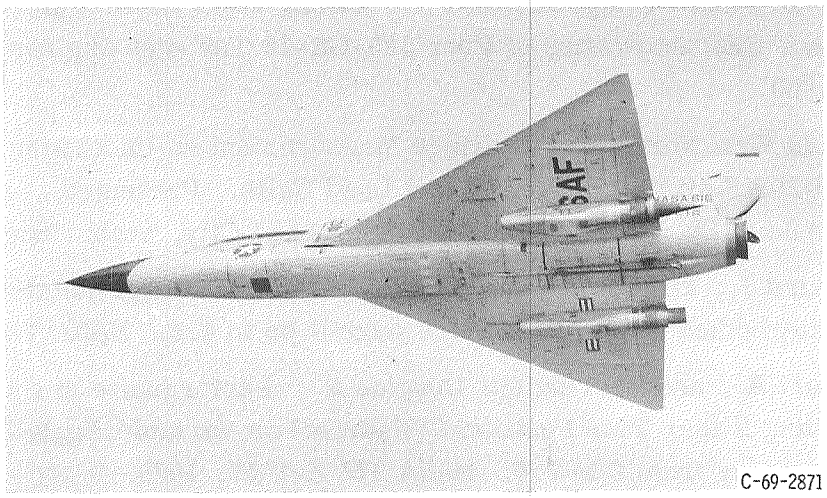

C-69-2871

Figure 1. - Modified F-106B aircraft in flight.

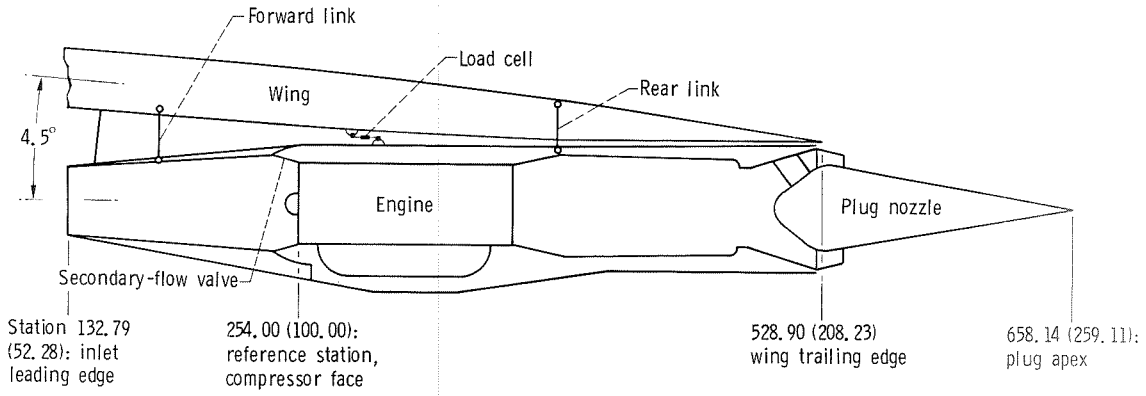

Figure 2. - Schematic of test installation. (All dimensions are in cm (in.).)

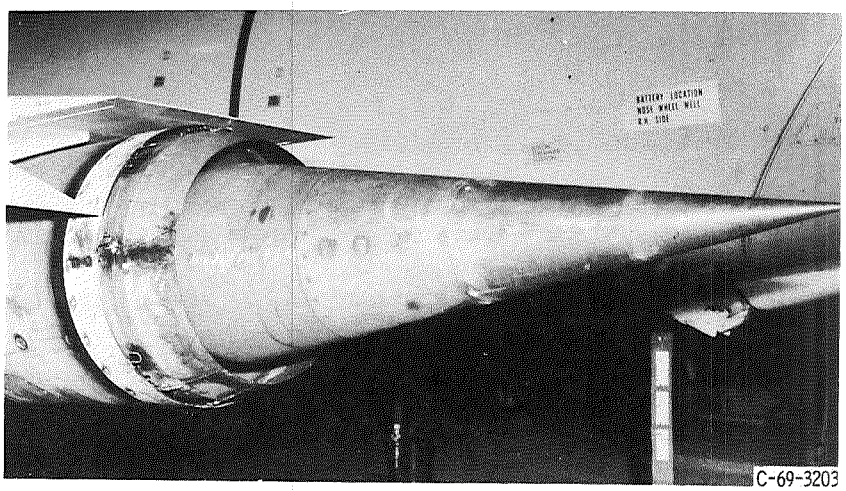

(a) Plug length, 100 percent.

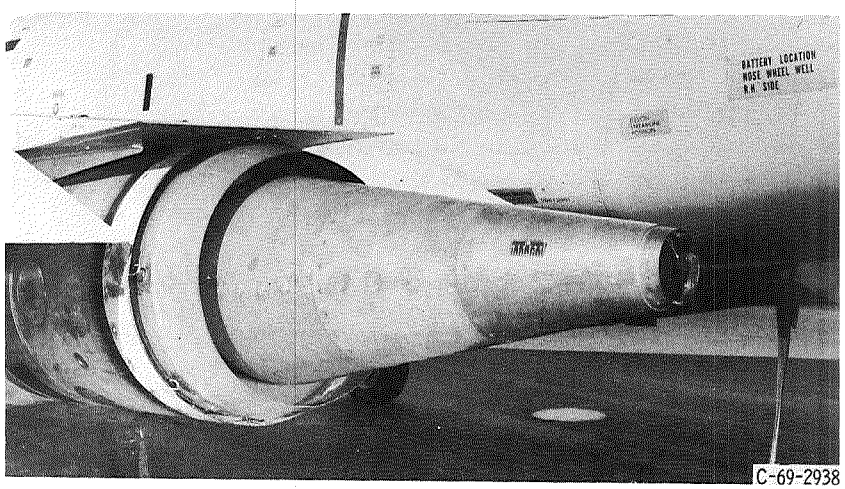

(b) Plug length, 73 percent (open base).

Figure 3. - Cylindrical nacelle assembly (shroud extension, $x/\ell = -0.120$).

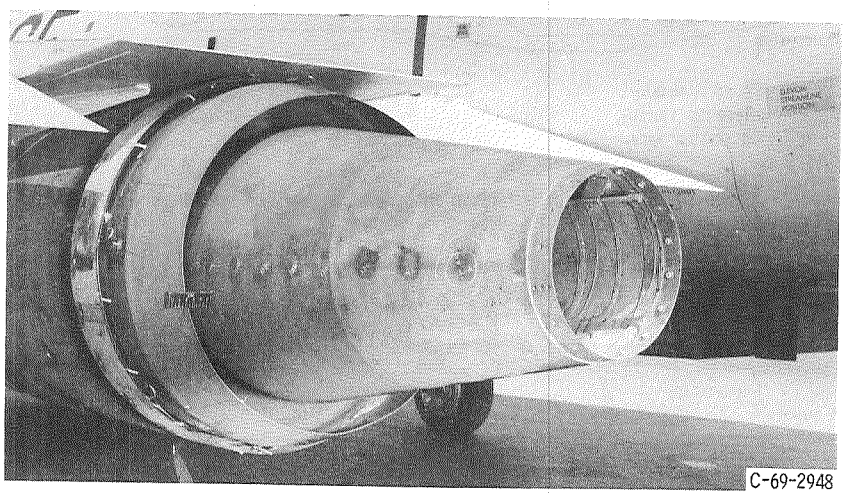

(c) Plug length, 48 percent (open base).

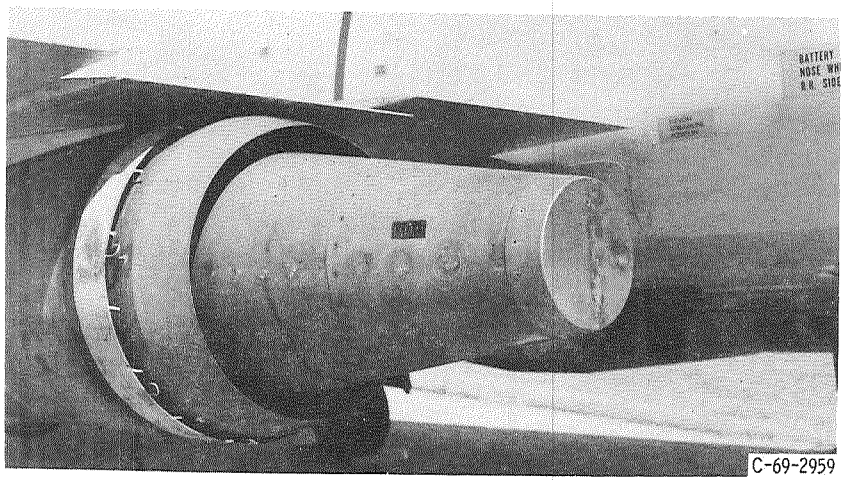

(d) Plug length, 50 percent (closed base).

Figure 3. - Concluded.

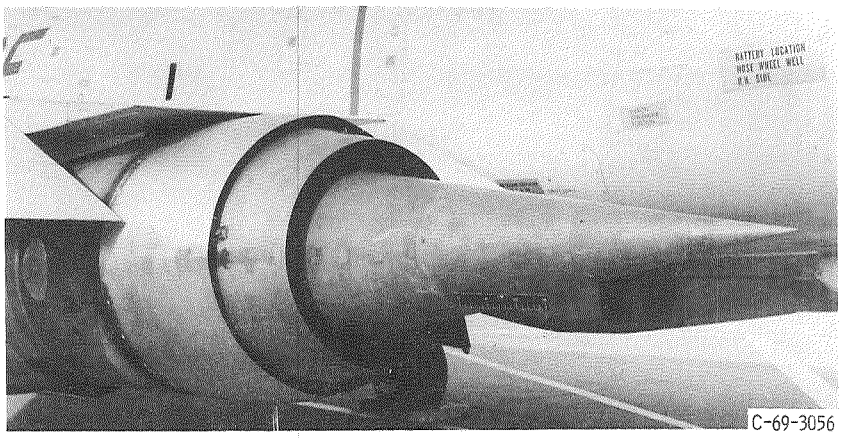

(a) Shroud extension, $x'/l' = -0.171$.

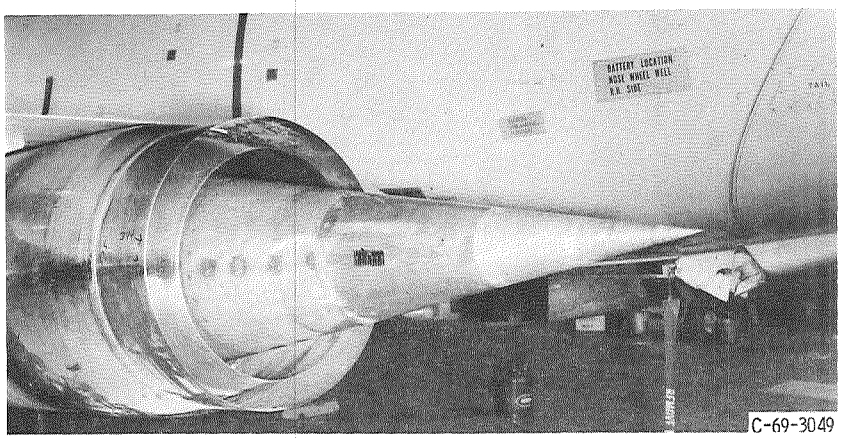

(b) Shroud extension, $x'/l' = 0.005$.

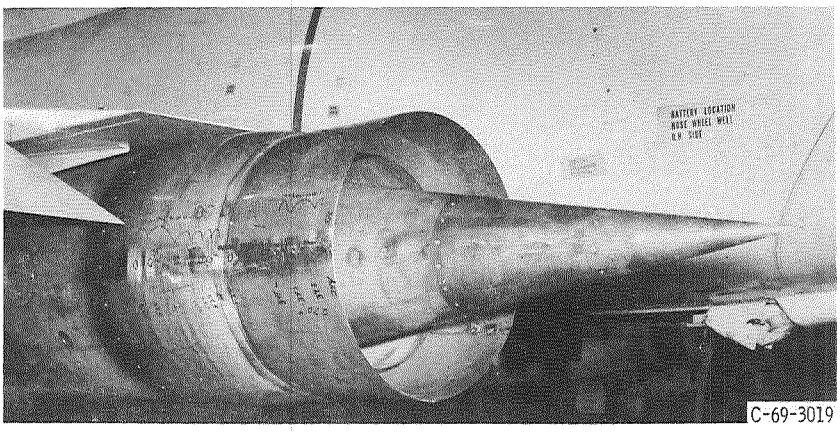

(c) Shroud extension, $x'/l' = 0.177$.

Figure 4. - Boattailed nacelle assembly. Plug length, 100 percent.

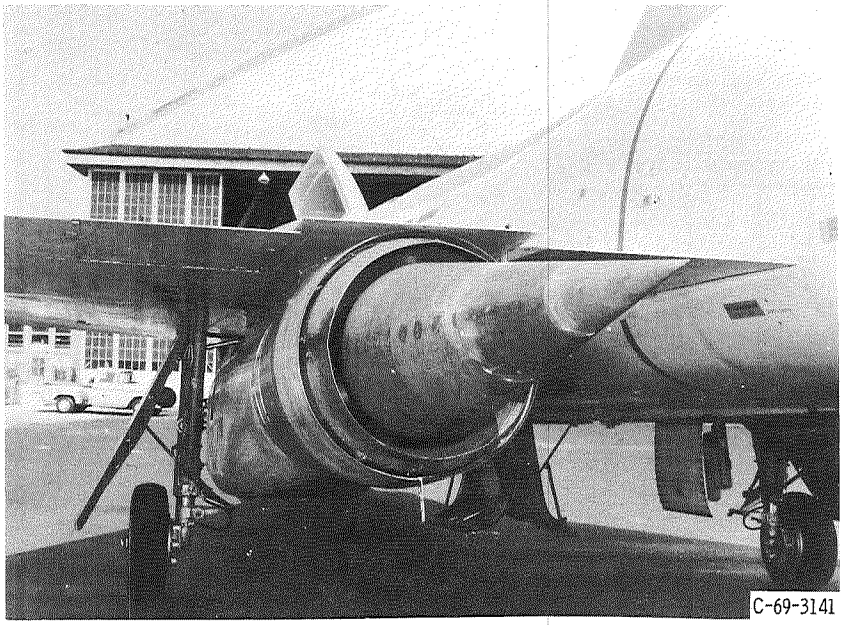

(a) Three-quarter aft view.

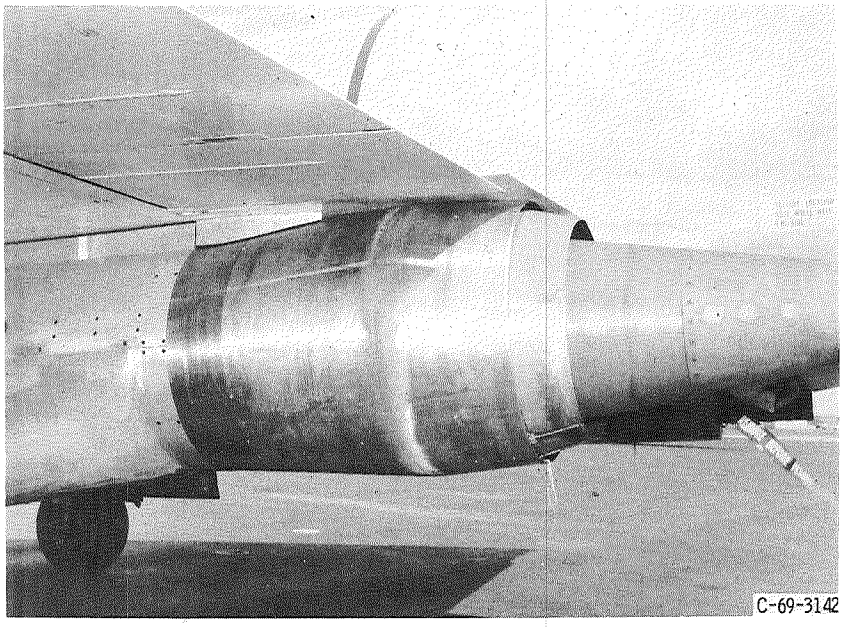

(b) Side view.

Figure 5. - Tapered nacelle assembly (shroud extension, $x/l = -0.08$).

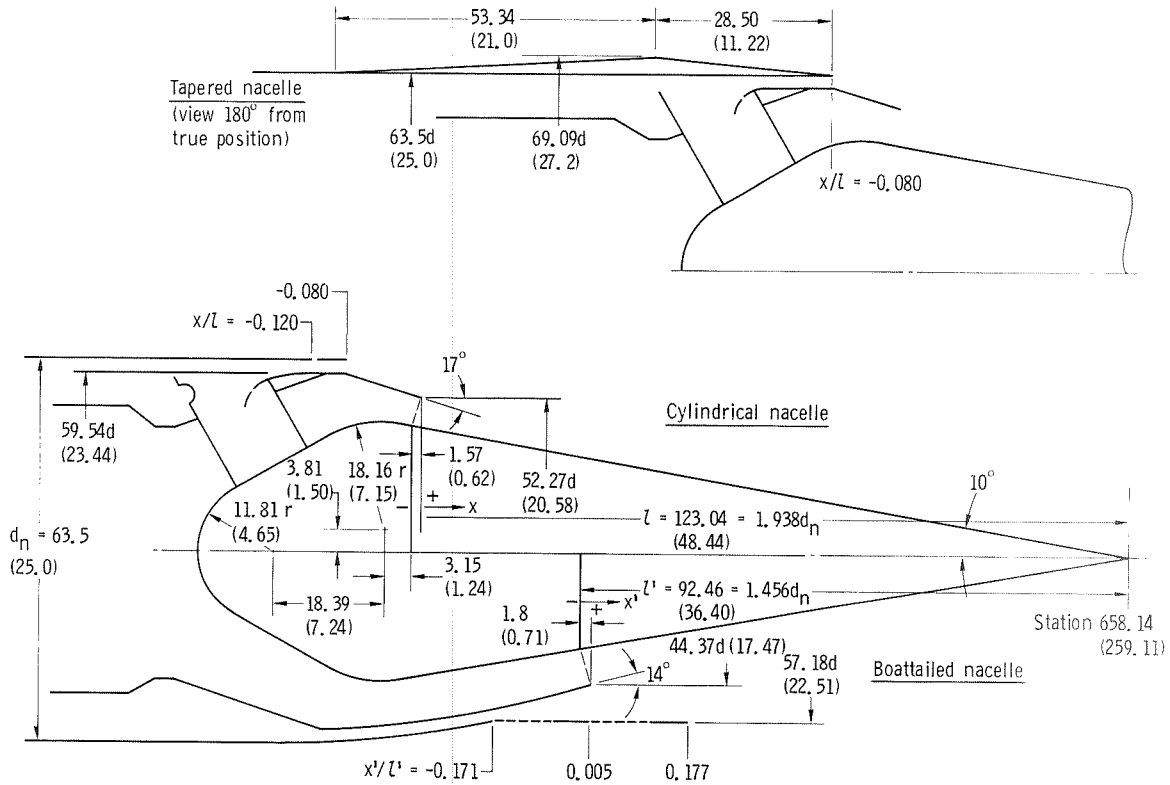

Figure 6. - Plug nozzle dimensions. (All dimensions are in cm (in.).)

x'/l'	r/l'
-0.613	0.342
-.437	.342
-.409	.341
-.382	.340
-.355	.338
-.327	.336

x'/l'	r/l'
-0.300	0.333
-.272	.330
-.245	.325
-.217	.320
-.190	.314
-.171	.309

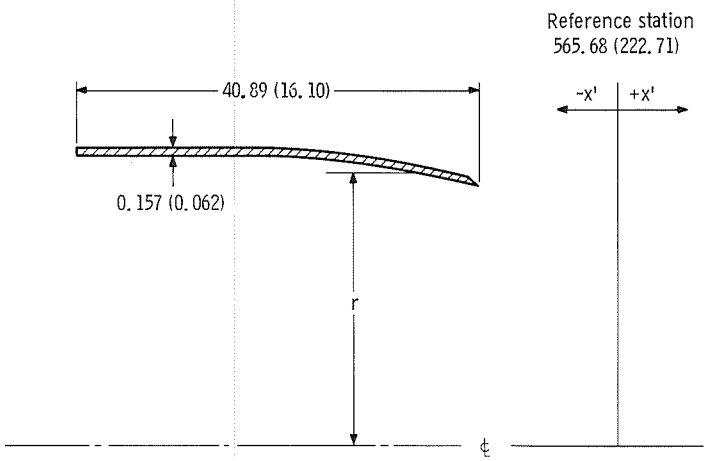

Figure 7. - Coordinates of boattailed nacelle. Shroud extension, $x'/l' = -0.171$; plug length, $l' = 92.46$ centimeters (36.40 in.) (All dimensions are in cm (in.).)

x'/l'	r/l'
-0.429	0.322
-.402	.321
-.374	.320
-.347	.318
-.320	.315
-.292	.312

x'/l'	r/l'	
-0.265	0.308	
-.237	.303	
-.210	.298	
-.182	.291	
-.165	.288	Straight line
.020	.242	

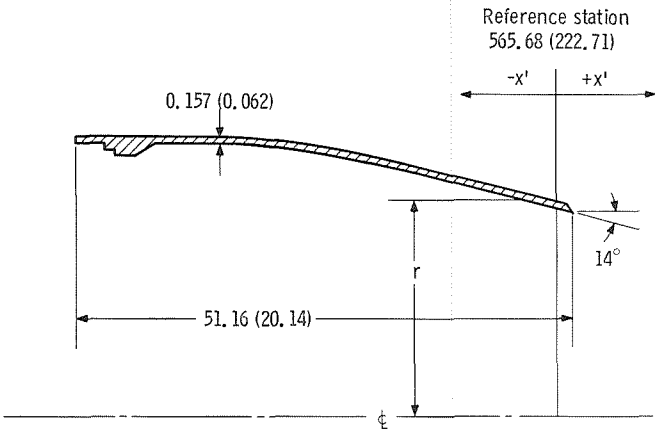

Figure 8. - Coordinates of 14° rounded primary flap. Plug length, l' = 92.46 centimeters (36.40 in.). (All dimensions are in cm (in.).)

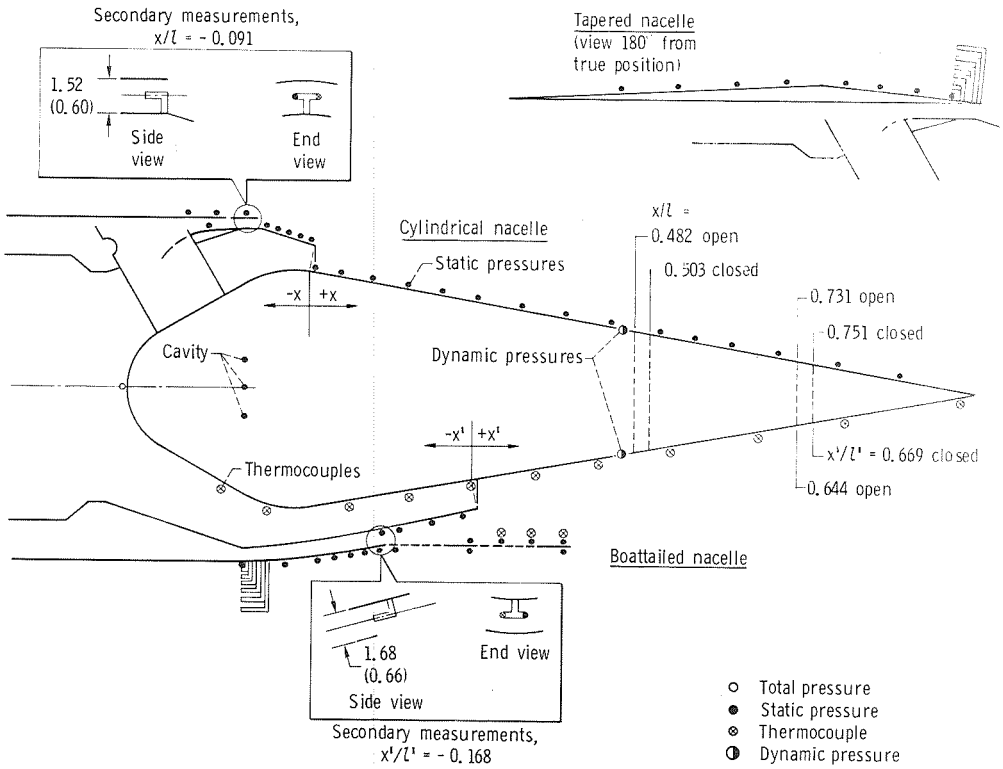

(a) Shrouds and plug truncations.

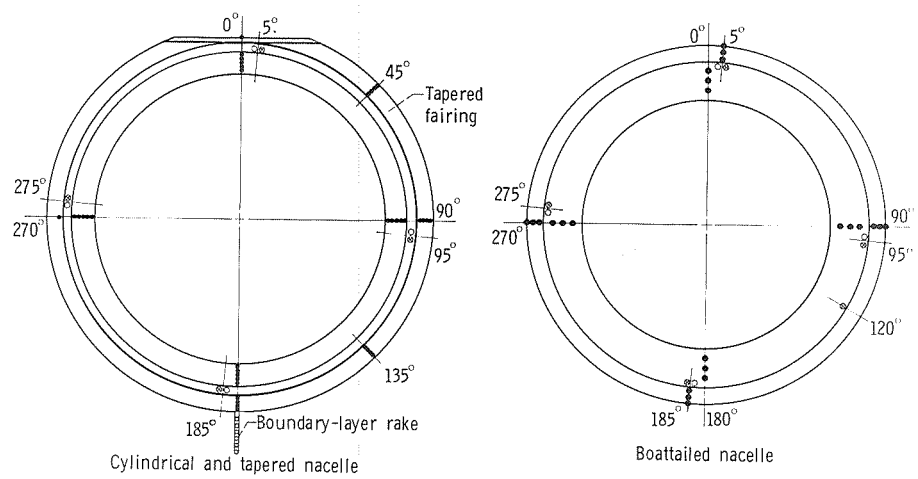

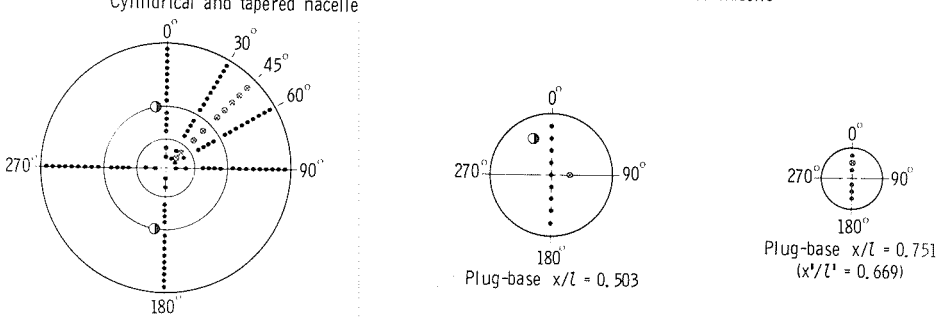

(b) Instrumentation, looking upstream.

Figure 9. - Plug nozzle instrumentation, shrouds, and plug truncations. (All dimensions are in cm (in.).)

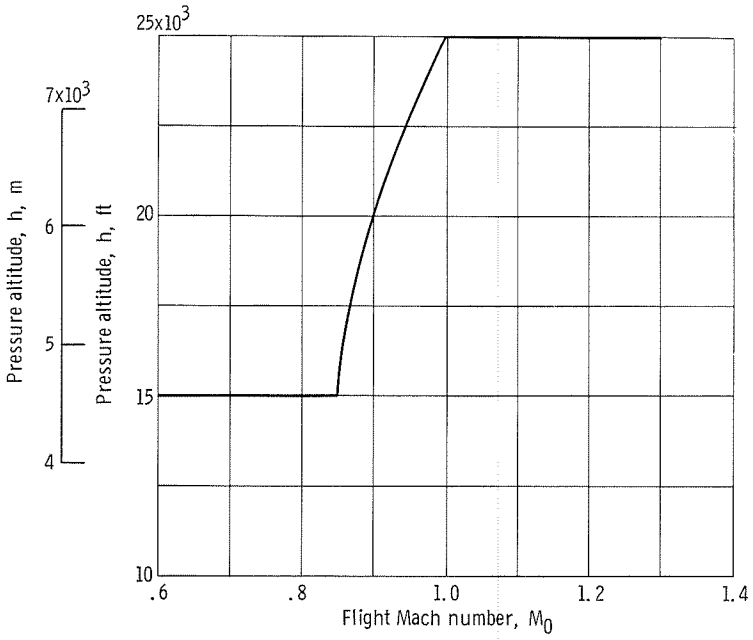

Figure 10. - Nominal flight test altitude - Mach number profile.

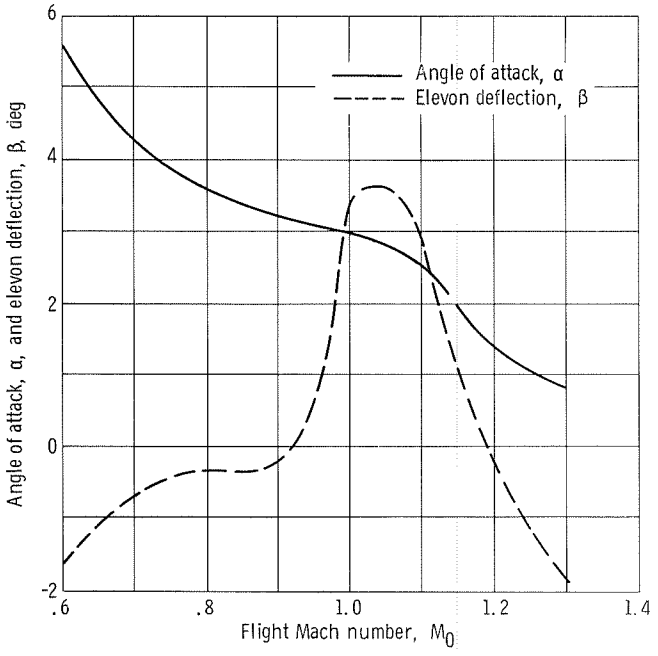

Figure 11. - Angle of attack and elevon deflection over flight test profile.

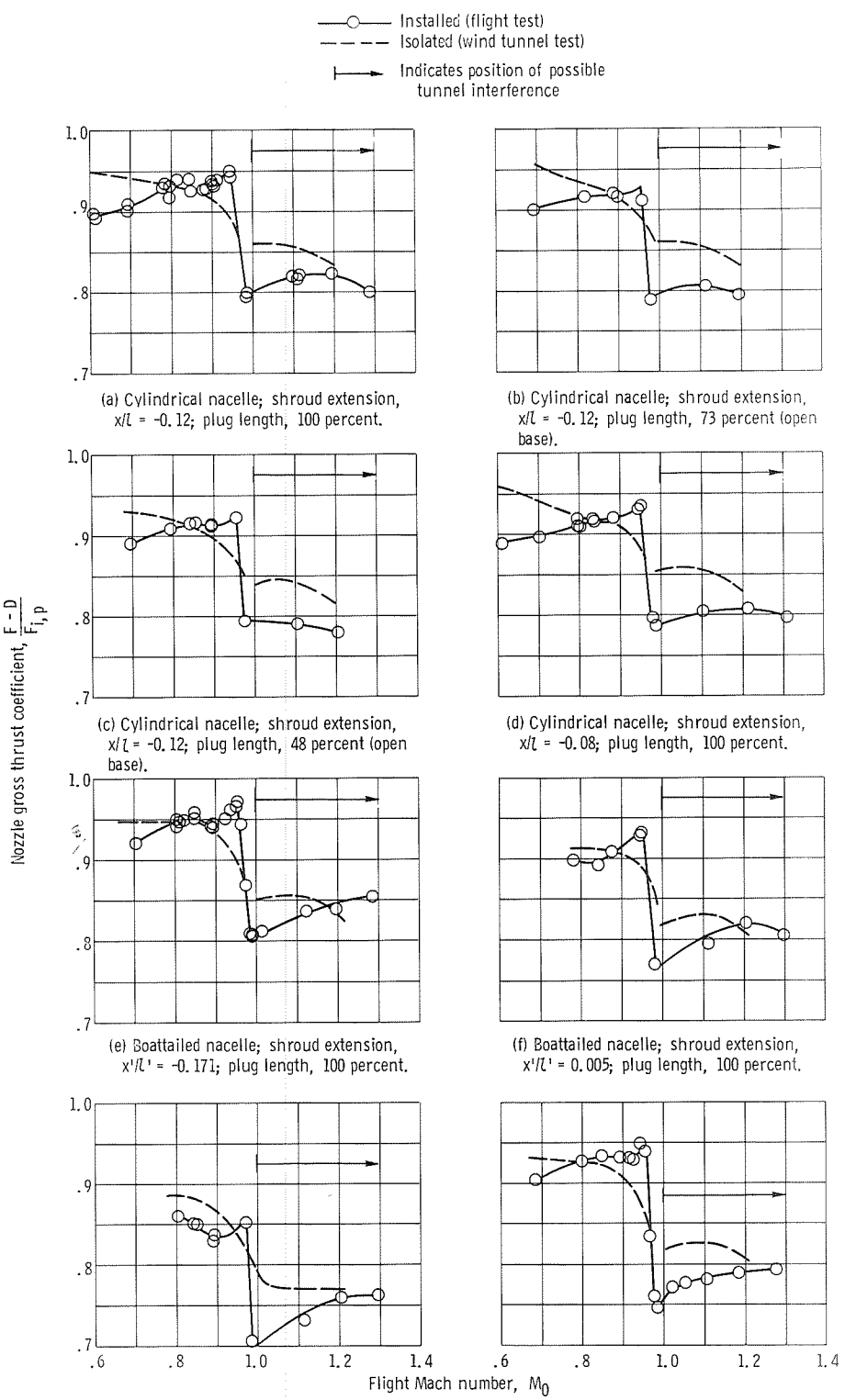

(a) Cylindrical nacelle; shroud extension, $x/\ell = -0.12$; plug length, 100 percent.

(b) Cylindrical nacelle; shroud extension, $x/\ell = -0.12$; plug length, 73 percent (open base).

(c) Cylindrical nacelle; shroud extension, $x/\ell = -0.12$; plug length, 48 percent (open base).

(d) Cylindrical nacelle; shroud extension, $x/\ell = -0.08$; plug length, 100 percent.

(e) Boattailed nacelle; shroud extension, $x'/\ell' = -0.171$; plug length, 100 percent.

(f) Boattailed nacelle; shroud extension, $x'/\ell' = 0.005$; plug length, 100 percent.

(g) Boattailed nacelle; shroud extension, $x'/\ell' = 0.177$; plug length, 100 percent.

(h) Tapered nacelle; shroud extension, $x/\ell = -0.08$; plug length, 100 percent. (Nozzle charged for aft cone force.)

Figure 12. - Installation effect on nozzle performance. Nominal corrected secondary weight flow, $\omega\sqrt{\theta} = 0.03$.

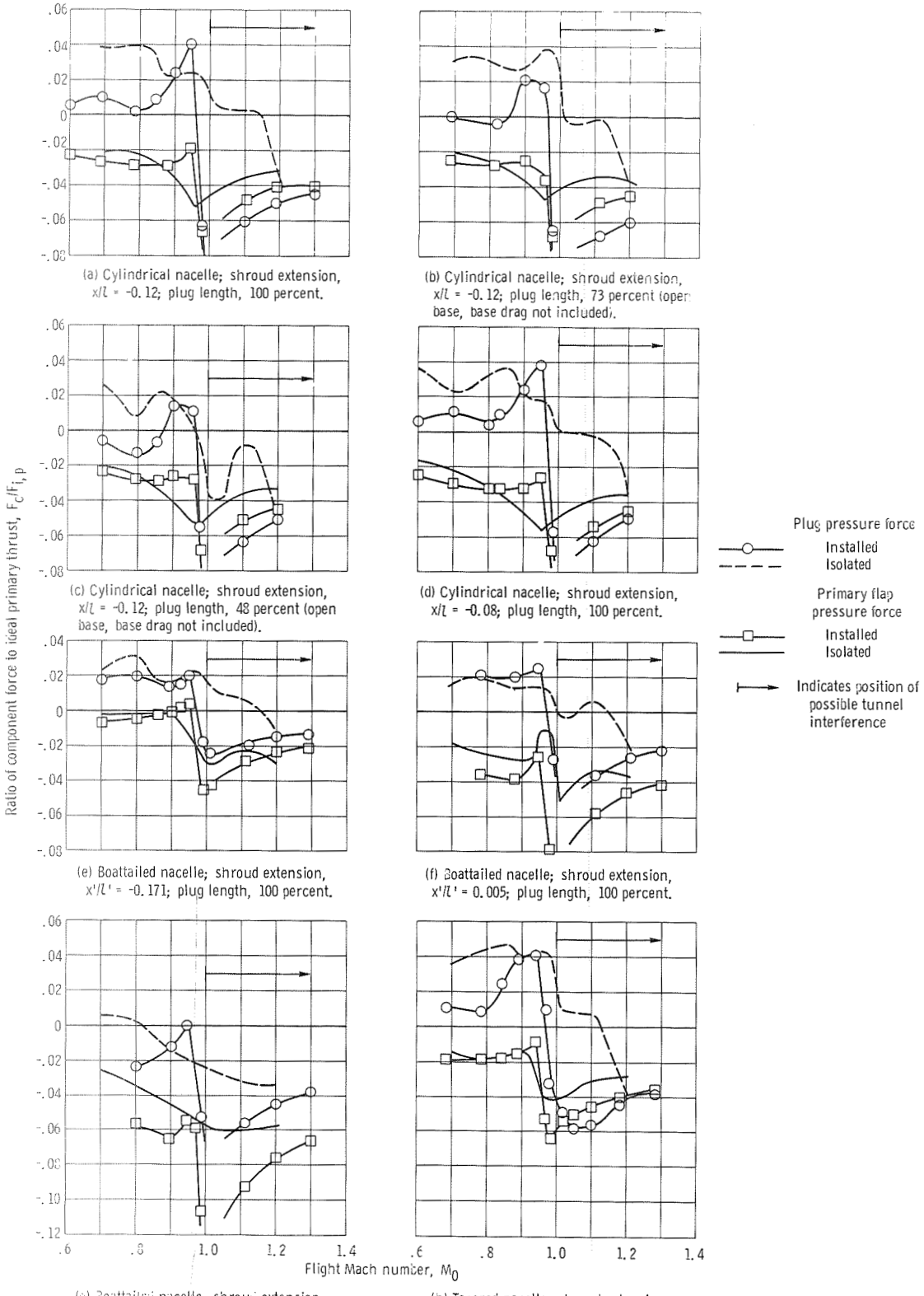

(a) Cylindrical nacelle; shroud extension, x/ℓ = -0.12; plug length, 100 percent.

(b) Cylindrical nacelle; shroud extension, x/ℓ = -0.12; plug length, 73 percent (open base, base drag not included).

(c) Cylindrical nacelle; shroud extension, x/ℓ = -0.12; plug length, 48 percent (open base, base drag not included).

(d) Cylindrical nacelle; shroud extension, x/ℓ = -0.08; plug length, 100 percent.

(e) Boattailed nacelle; shroud extension, x'/ℓ' = -0.171; plug length, 100 percent.

(f) Boattailed nacelle; shroud extension, x'/ℓ' = 0.005; plug length, 100 percent.

(g) Boattailed nacelle; shroud extension, x'/ℓ' = 0.177; plug length, 100 percent.

(h) Tapered nacelle; shroud extension, x/ℓ = -0.08; plug length, 100 percent.

Figure 13. - Component force breakdown of installed and isolated plug nozzle. Nominal corrected secondary weight flow, $\omega\sqrt{\theta}$ = 0.03.

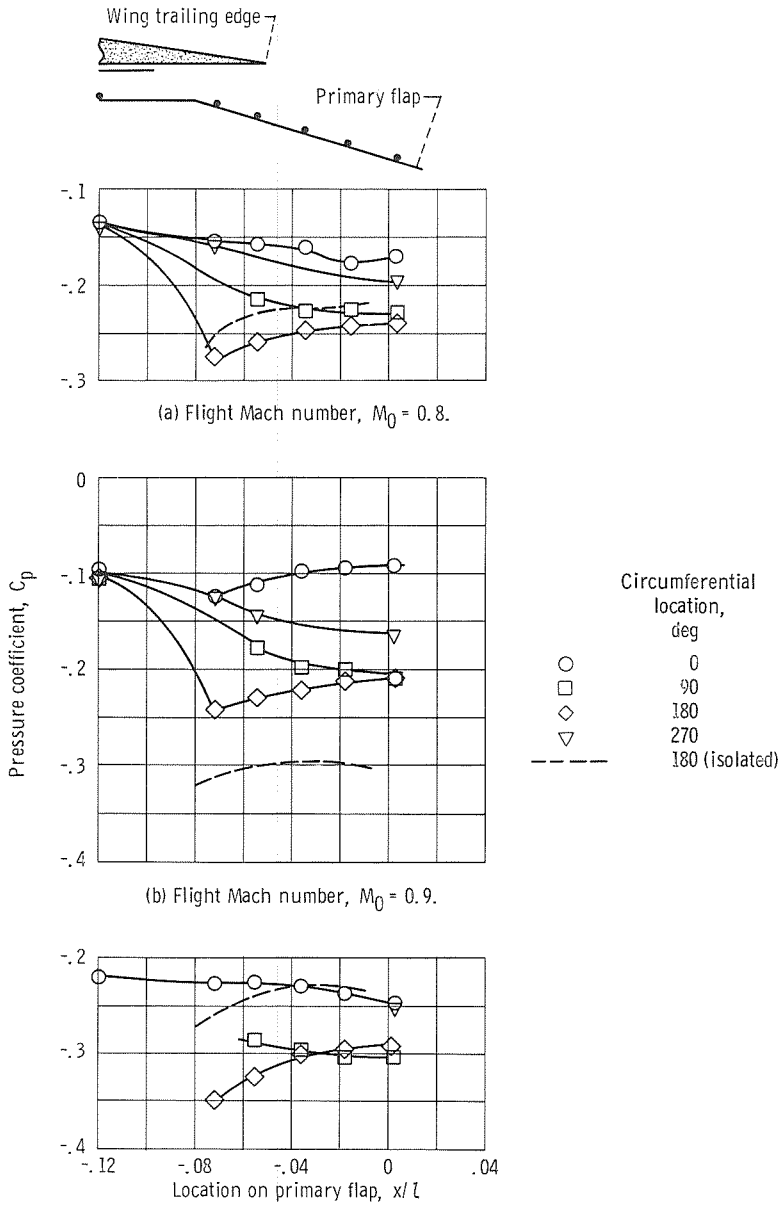

(a) Flight Mach number, $M_0 = 0.8$.

(b) Flight Mach number, $M_0 = 0.9$.

(c) Flight Mach number, $M_0 = 1.1$.

Figure 14. - Installed and isolated pressure distribution for cylindrical nacelle (shroud extension, $x/l = -0.12$). Military power; plug length, 100 percent; corrected secondary weight flow, $\omega\sqrt{\tau} = 0.03$.

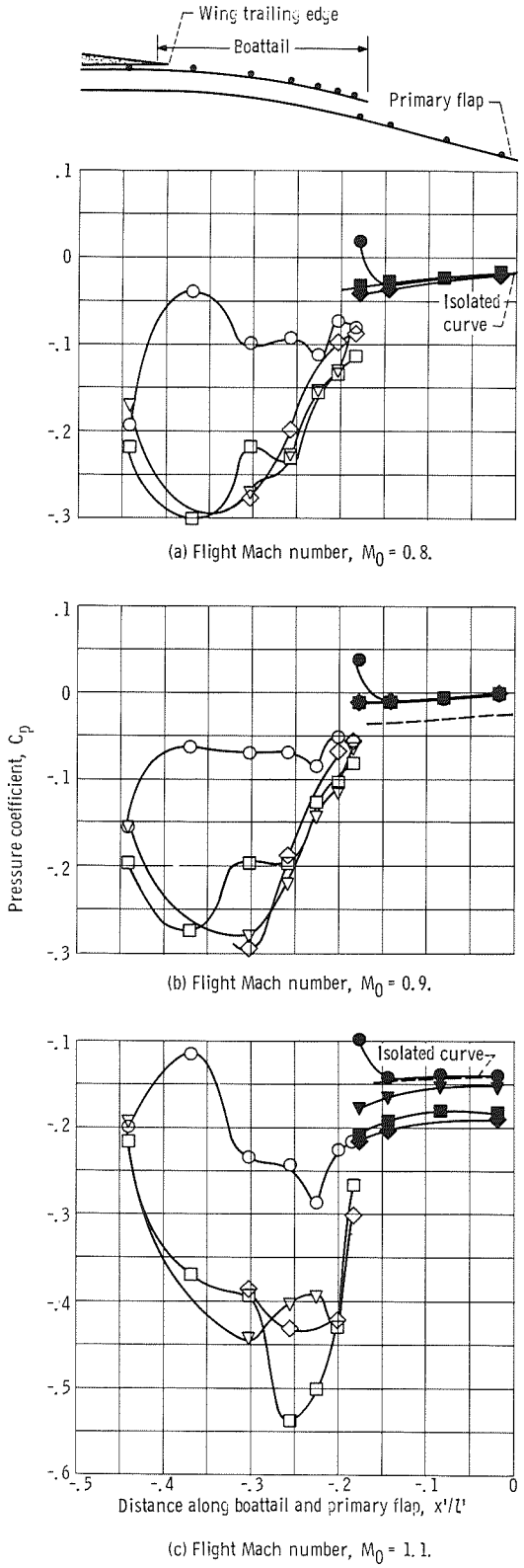

Figure 15. - Installed and isolated pressure distribution for boattailed nacelle (shroud extension, $x'/l' = -0.171$). Military power; plug length, 100 percent; corrected secondary weight flow, $\omega\sqrt{\tau} = 0.03$.

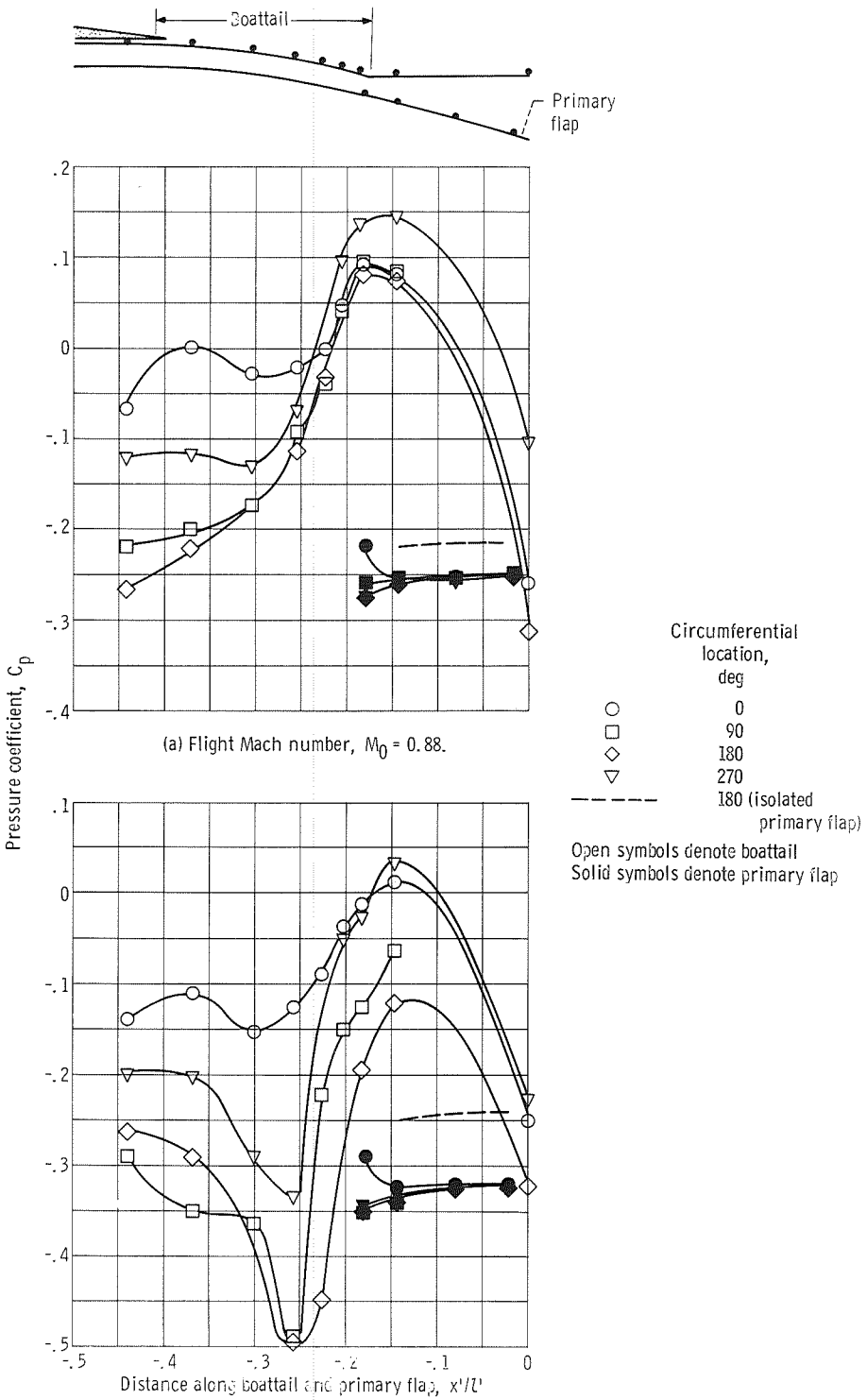

Figure 16. - Installed and isolated pressure distribution for boattailed nacelle (shroud extension, $x'/l' = 0.005$). Military power; plug length, 100 percent; corrected secondary weight flow, $w\sqrt{\theta}/\delta = 0.03$.

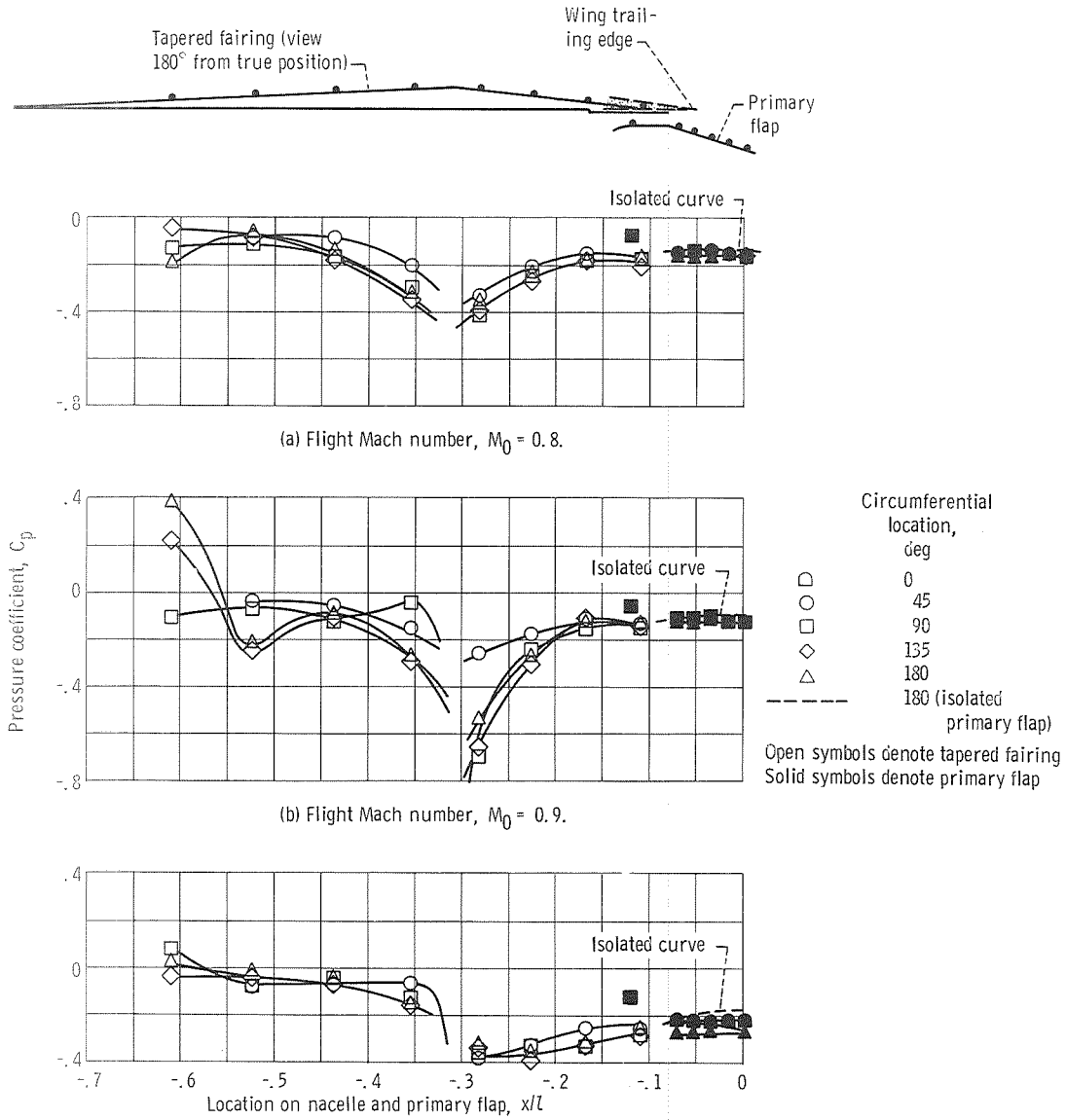

Figure 17. - Installed and isolated pressure distribution for tapered nacelle (shroud extension, x/l = -0.08). Military power; plug length, 100 percent; corrected secondary weight flow, $\omega\sqrt{\theta}/\delta$ = 0.03.

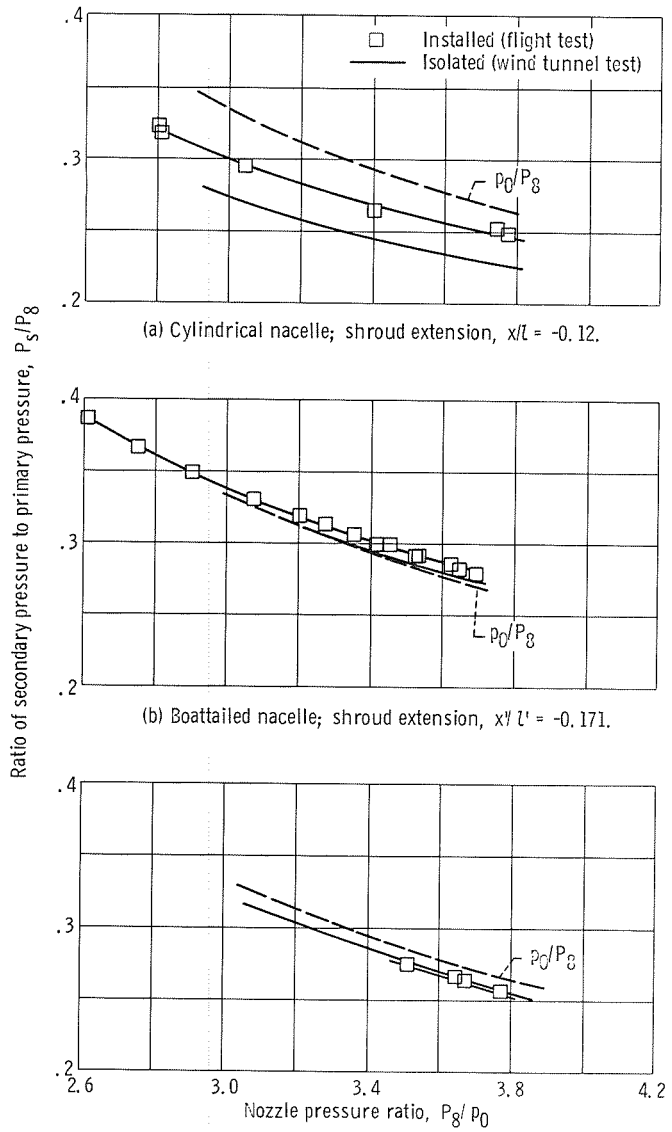

(a) Cylindrical nacelle; shroud extension, $x/l = -0.12$.

(b) Boattailed nacelle; shroud extension, $x/l' = -0.171$.

(c) Tapered nacelle; shroud extension, $x/l = -0.08$.

Figure 18. - Effect of installation on pumping characteristics. Plug length, 100 percent; flight Mach number, $M_0 = 0.9$; corrected secondary weight flow, $\omega\sqrt{\tau} = 0.03$.

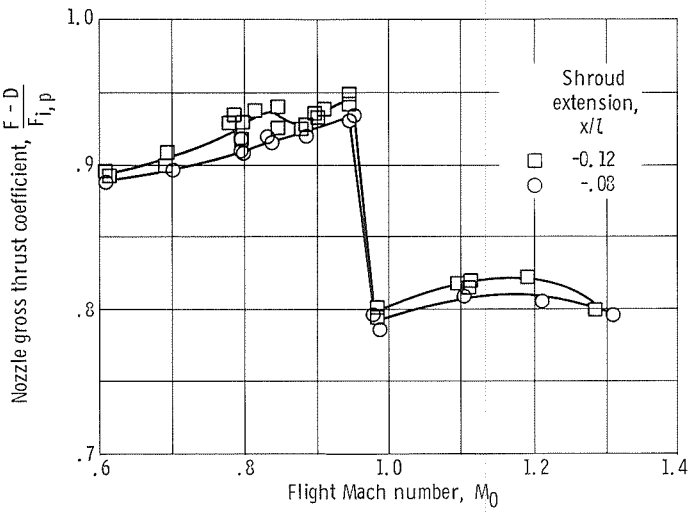

Figure 19. - Effect of shroud extension on performance of cylindrical nacelle. Plug length, 100 percent; military power; corrected secondary weight flow, $\omega\sqrt{\theta}$ = 0.03.

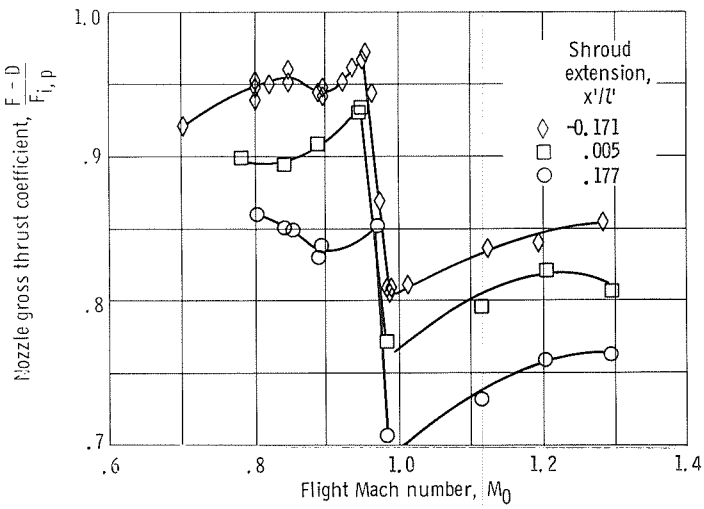

Figure 20. - Effect of shroud extension on performance of boattailed nacelle. Plug length, 100 percent; military power; corrected secondary weight flow, $\omega\sqrt{\theta}$ = 0.03.

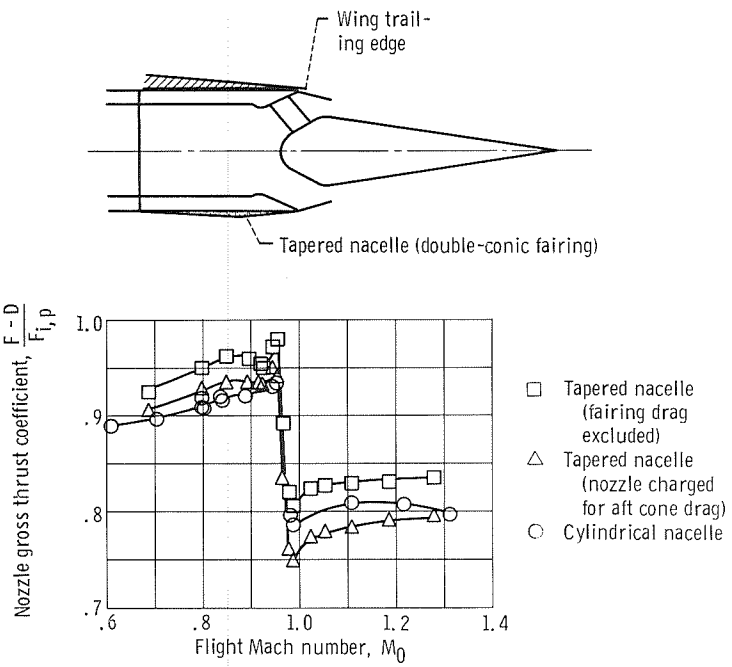

Figure 21. - Effect of nacelle geometry on plug nozzle performance. Shroud extension, $x/\ell = -0.08$; corrected secondary weight flow, $\omega\sqrt{\tau} = 0.03$.

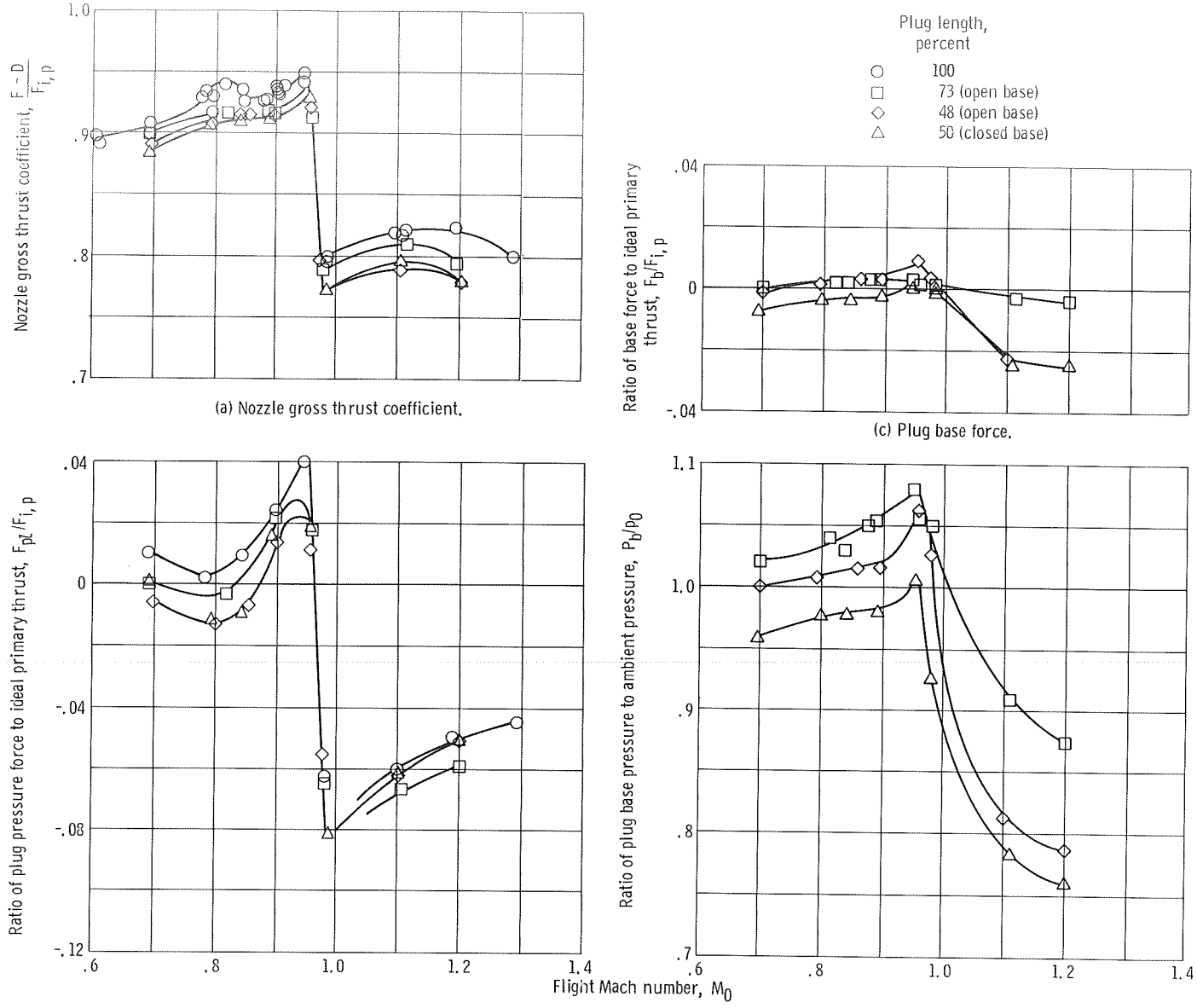

Figure 22. - Effect of plug truncation on cylindrical nacelle characteristics. Shroud extension, x/ℓ = -0.12; military power; corrected secondary weight flow, $\omega\sqrt{\tau}$ = 0.03.

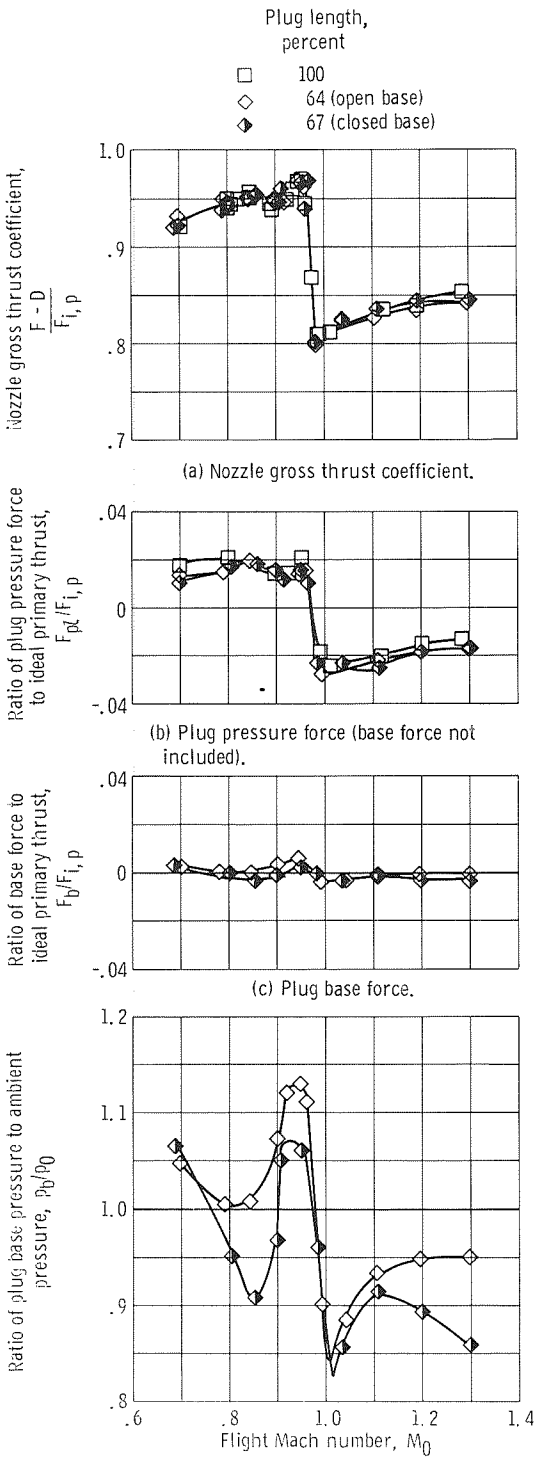

Figure 23. - Effect of plug truncation on boat-tailed nacelle characteristics. Shroud extension, $x/l' = -0.171$; military power; corrected secondary weight flow, $\omega\sqrt{\theta}/\delta = 0.03$

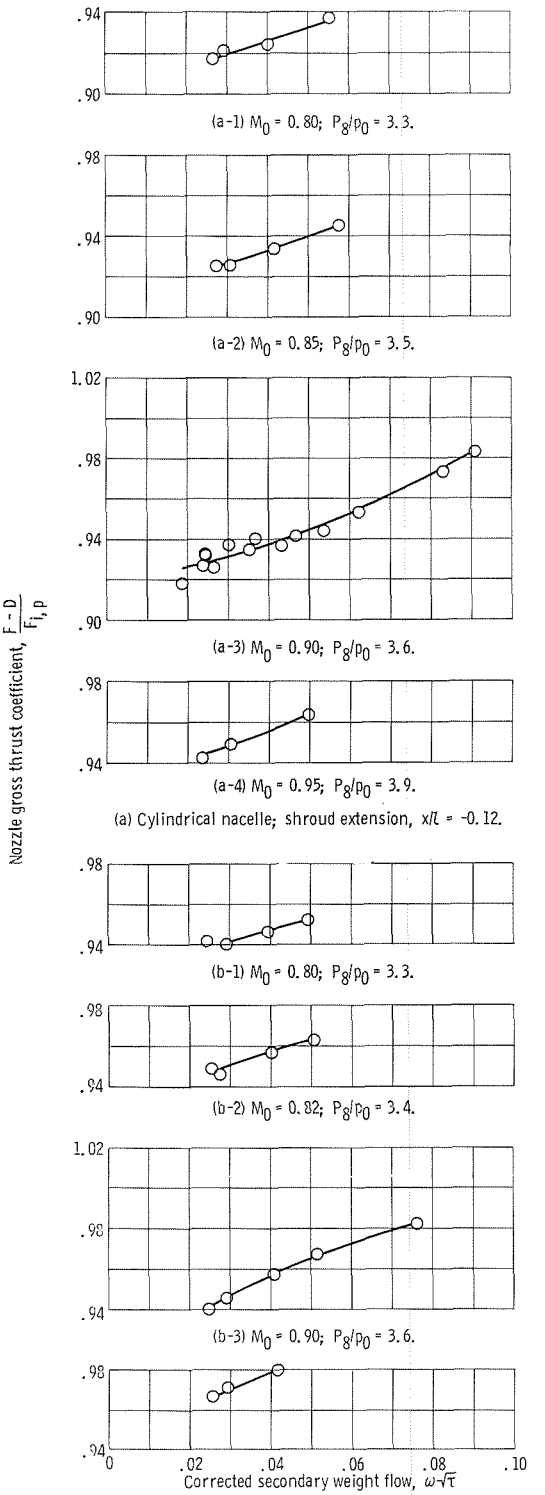

Figure 24. - Effect of secondary flow on nozzle gross thrust coefficient for various flight Mach numbers M_0 and nozzle pressure ratios P_8/p_0. Plug length, 100 percent; military power.

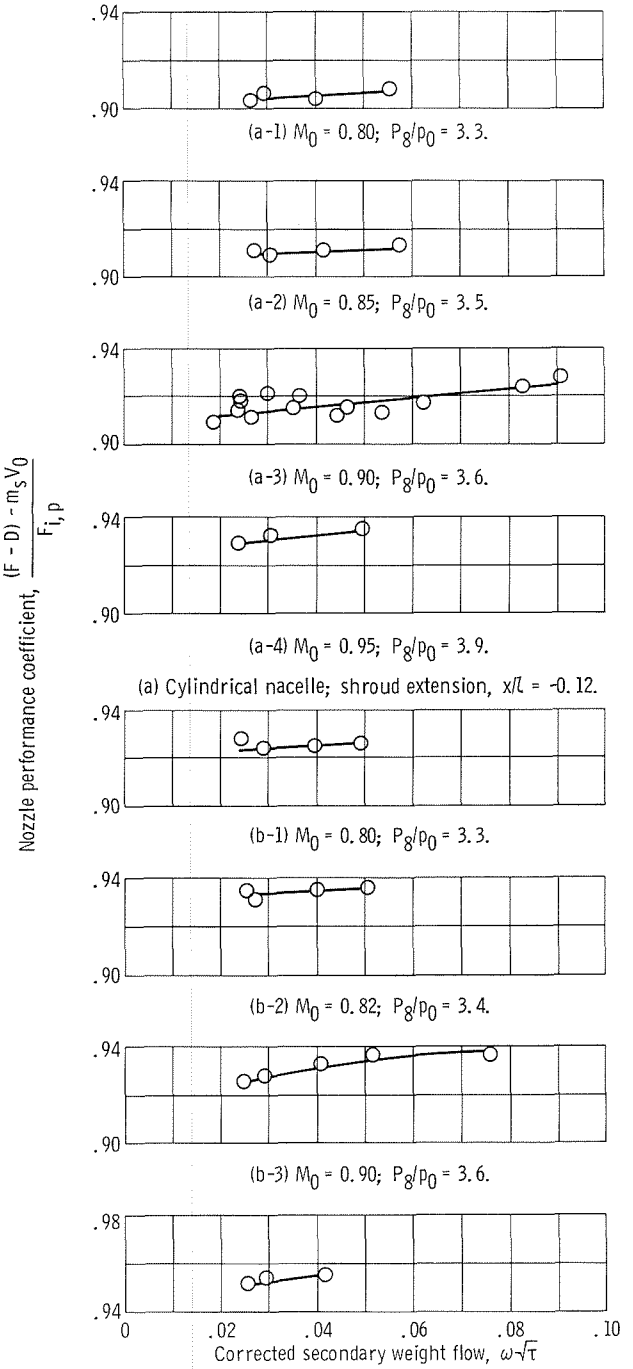

Figure 25. - Effect of secondary flow on nozzle performance coefficient for various flight Mach numbers M_0 and nozzle pressure ratios P_8/p_0. Plug length, 100 percent; military power.

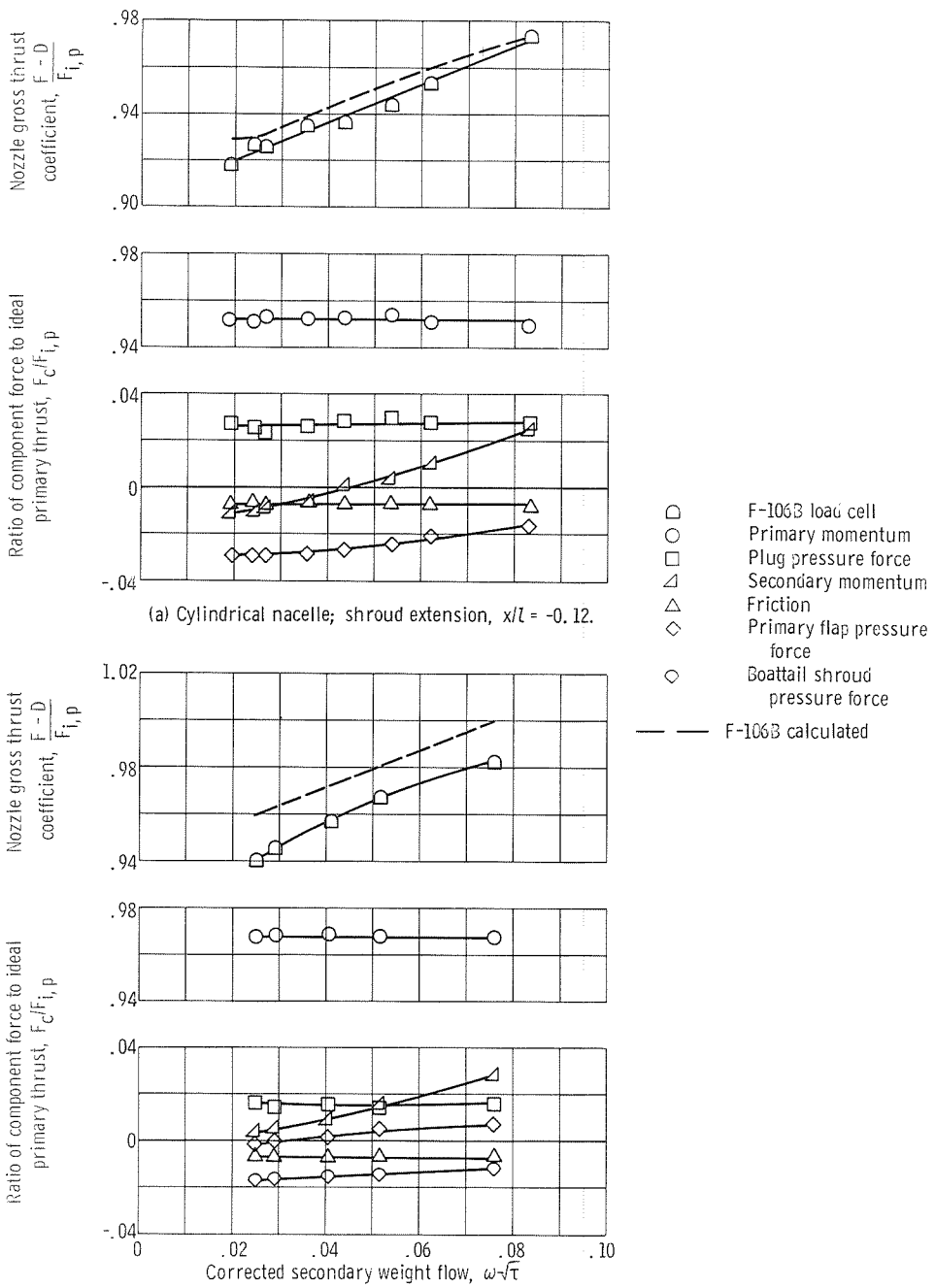

(a) Cylindrical nacelle; shroud extension, $x/l = -0.12$.

(b) Boattailed nacelle; shroud extension, $x'/l' = -0.171$.

Figure 26. - Effect of secondary flow on component forces. Flight Mach number, $M_0 = 0.9$; military power; plug length, 100 percent.

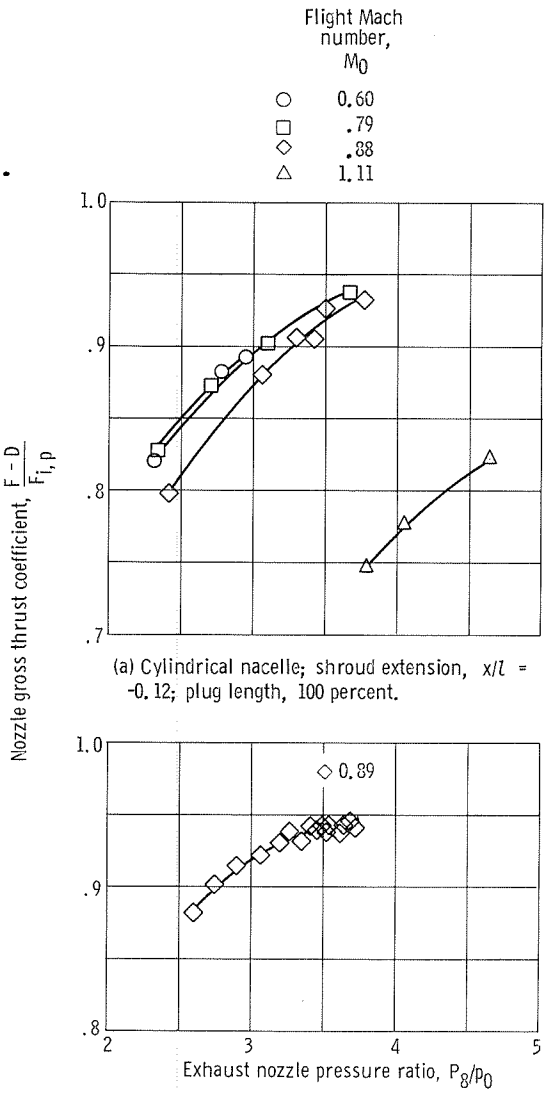

(a) Cylindrical nacelle; shroud extension, x/l = -0.12; plug length, 100 percent.

(b) Boattailed nacelle; shroud extension, x'/l' = -0.171; plug length, 100 percent.

Figure 27. - Effect of nozzle pressure ratio on nozzle gross thrust coefficient. Corrected secondary weight flow, $\omega\sqrt{\tau} = 0.03$.

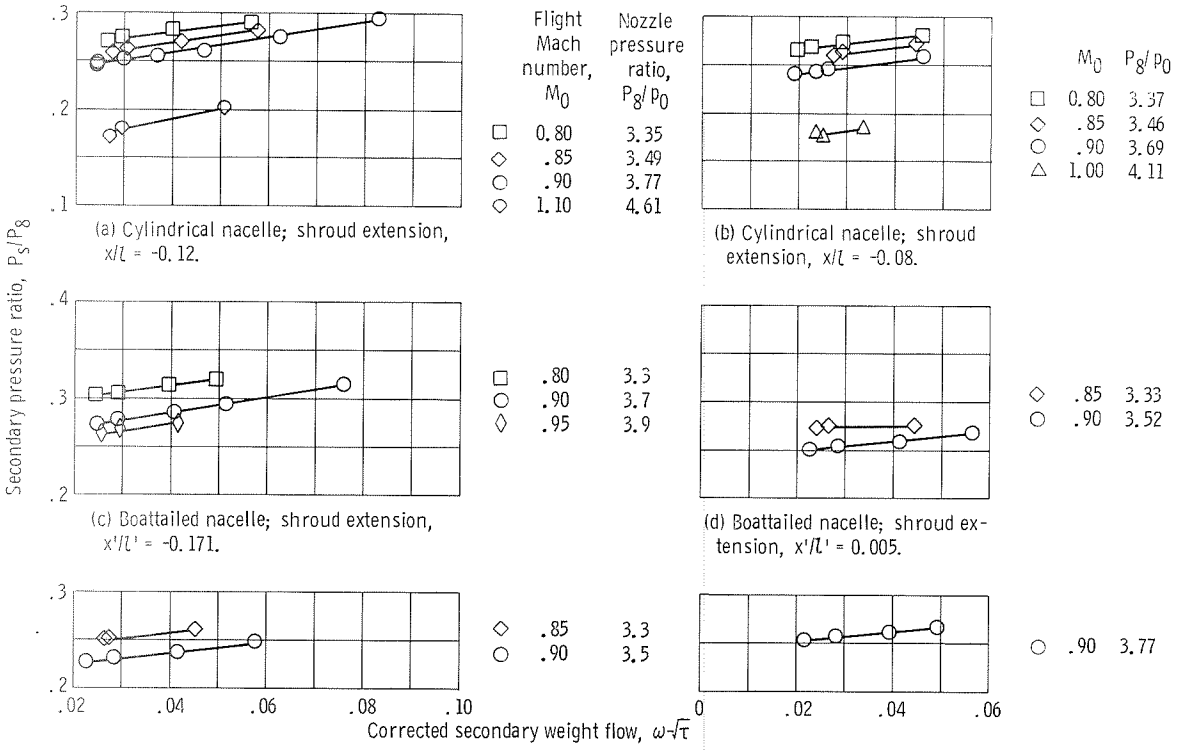

(a) Cylindrical nacelle; shroud extension, $x/\ell = -0.12$.

(b) Cylindrical nacelle; shroud extension, $x/\ell = -0.08$.

(c) Boattailed nacelle; shroud extension, $x'/\ell' = -0.171$.

(d) Boattailed nacelle; shroud extension, $x'/\ell' = 0.005$.

(e) Boattailed nacelle; shroud extension, $x'/\ell' = 0.177$.

(f) Tapered nacelle; shroud extension, $x/\ell = -0.08$.

Figure 28. - Pumping characteristics. Military power; plug length, 100 percent.

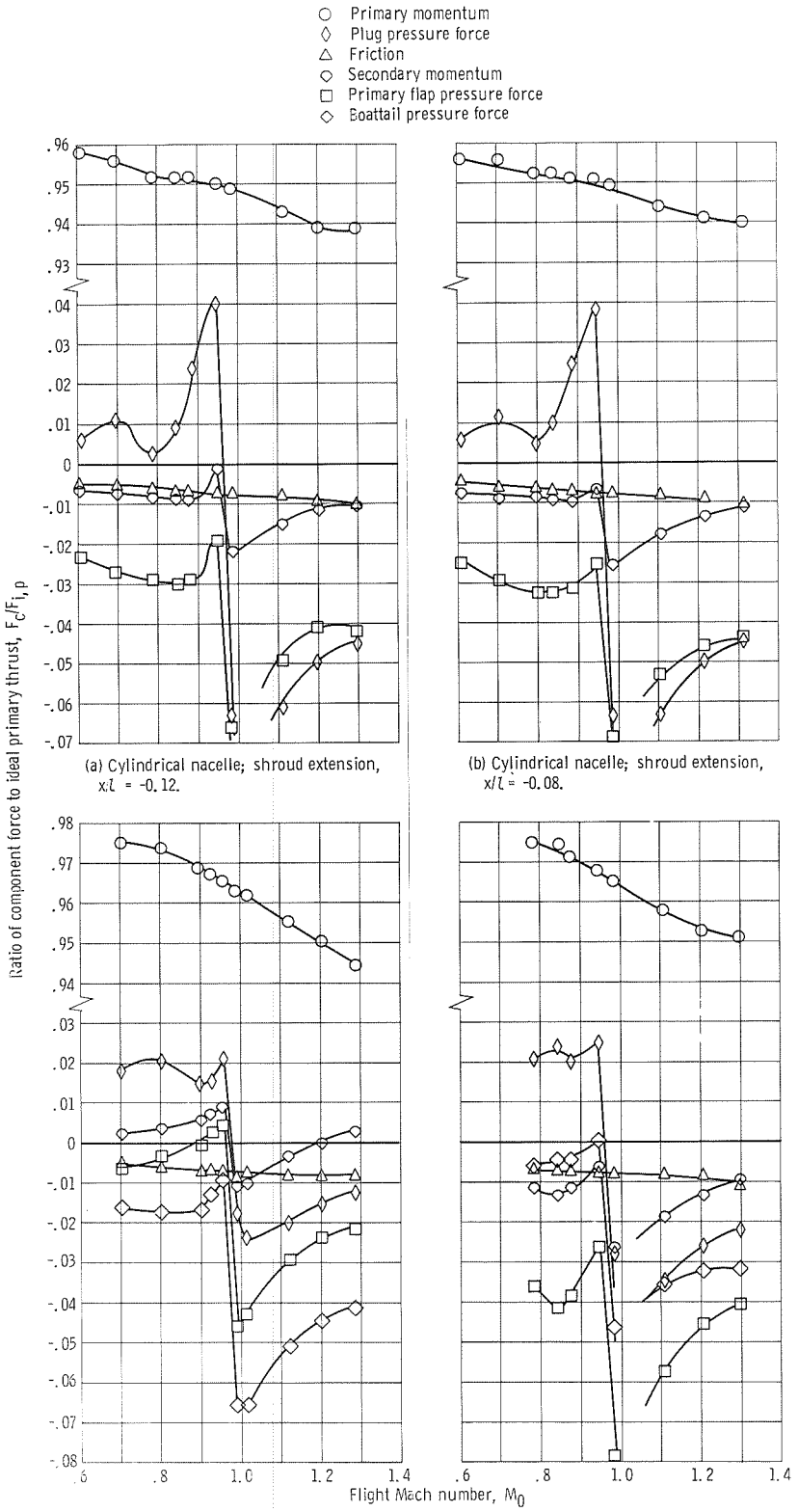

Figure 27. - Component force breakdown of 100-percent plug nozzle. Military power; nominal corrected secondary weight flow, $w_s\sqrt{\tau} = 0.03$.

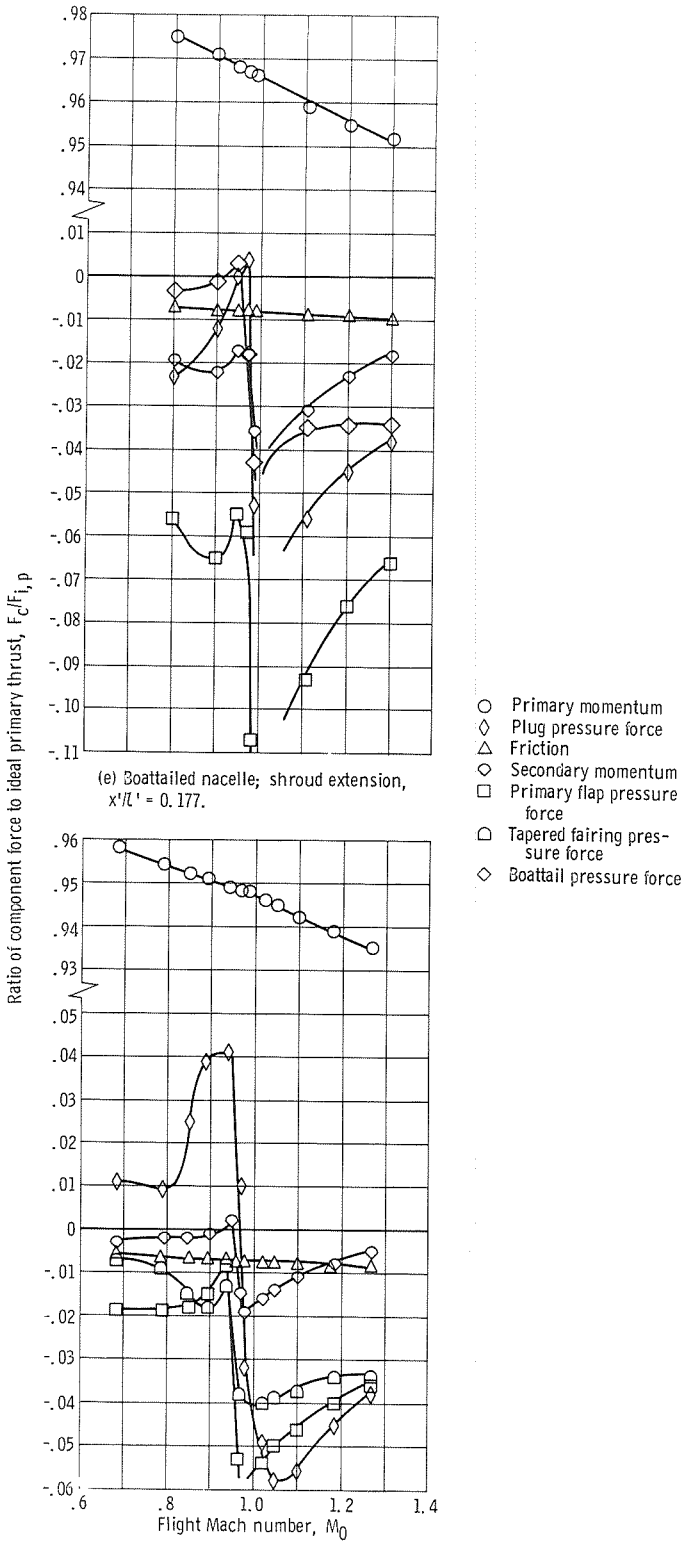

(e) Boattailed nacelle; shroud extension, $x'/l' = 0.177$.

(f) Tapered nacelle; shroud extension, $x/l = -0.08$.

Figure 29. - Concluded.

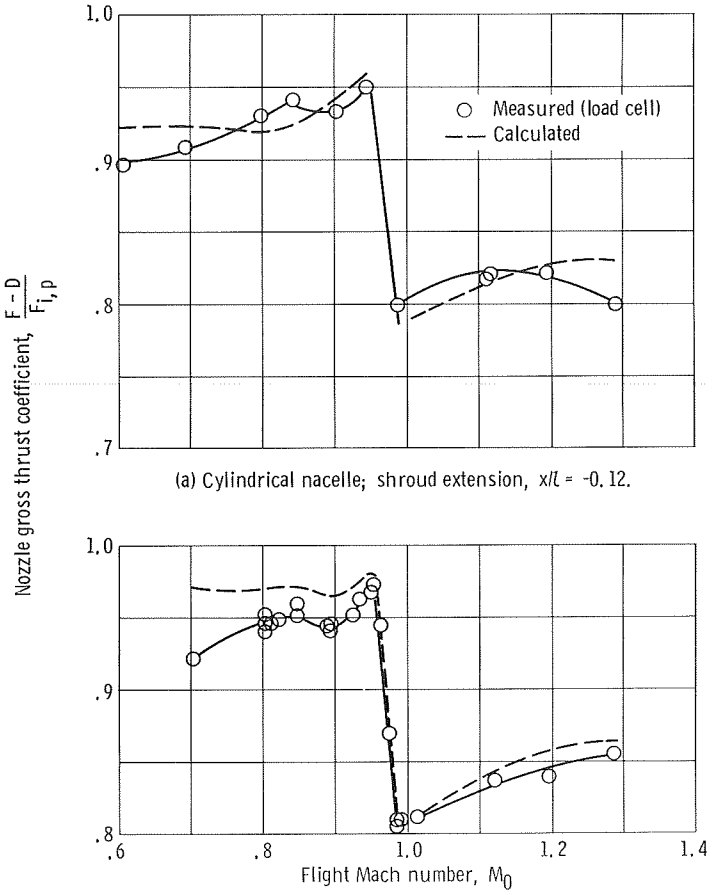

Figure 30. - Comparison of measured and calculated nozzle performance. Military power; plug length, 100 percent; corrected secondary weight flow, $\omega\sqrt{\tau} = 0.03$.

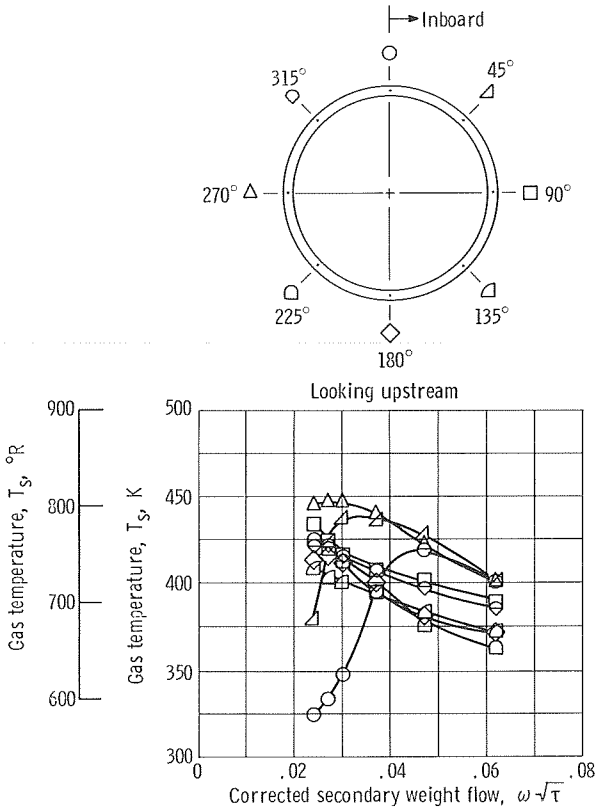

Figure 31. - Temperature profile in secondary exit plane. Flight Mach number, $M_0 = 0.9$; temperature at compressor inlet station, $T_2 = 304$ K (547° R); military power; plug length, 100 percent. Cylindrical nacelle; shroud extension, x/l = -0.12.

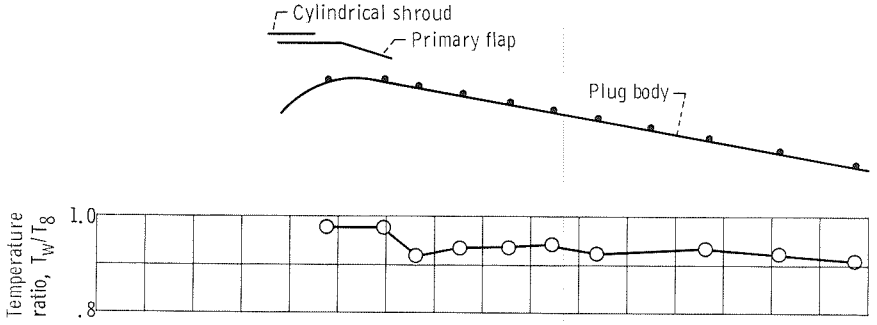

(a) Cylindrical nacelle; shroud extension, $x/\ell = -0.12$; flight Mach number, $M_0 = 0.88$; temperature at primary nozzle throat, $T_8 = 968$ K (1742° R).

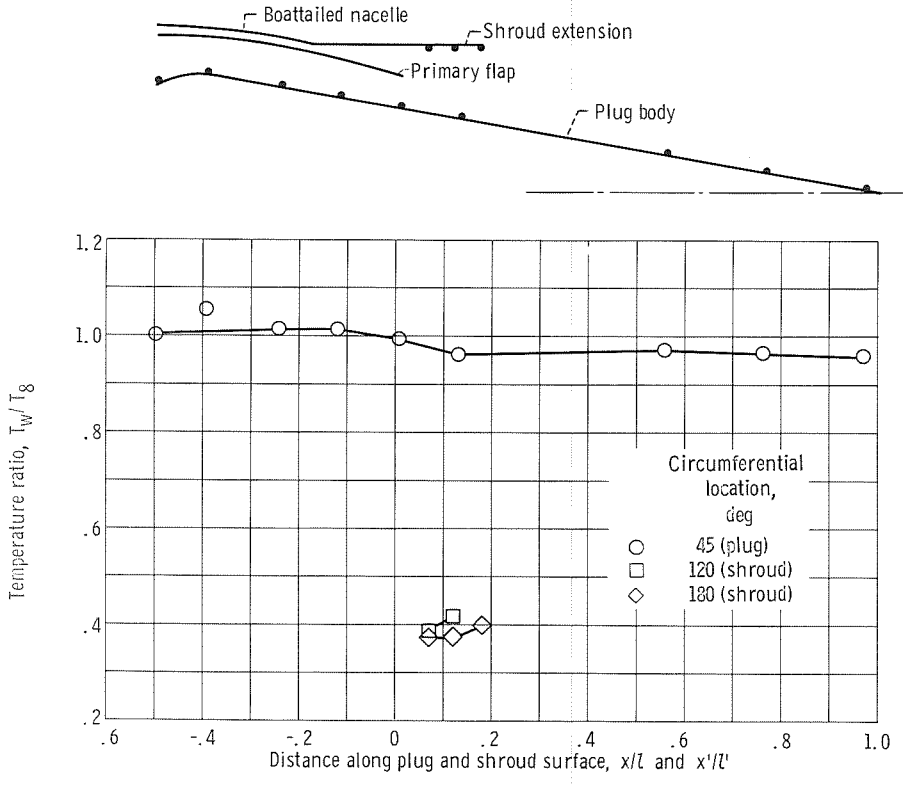

(b) Boattailed nacelle; shroud extension, $x'/\ell' = 0.177$; flight Mach number, $M_0 = 0.9$; temperature at primary nozzle throat, $T_8 = 892$ K (1606° R).

Figure 32. - Temperature distribution along plug and shroud surface. Military power; plug length, 100 percent; meridian angle, 45°; corrected secondary weight flow, $w\sqrt{\theta}/\delta = 0.03$.

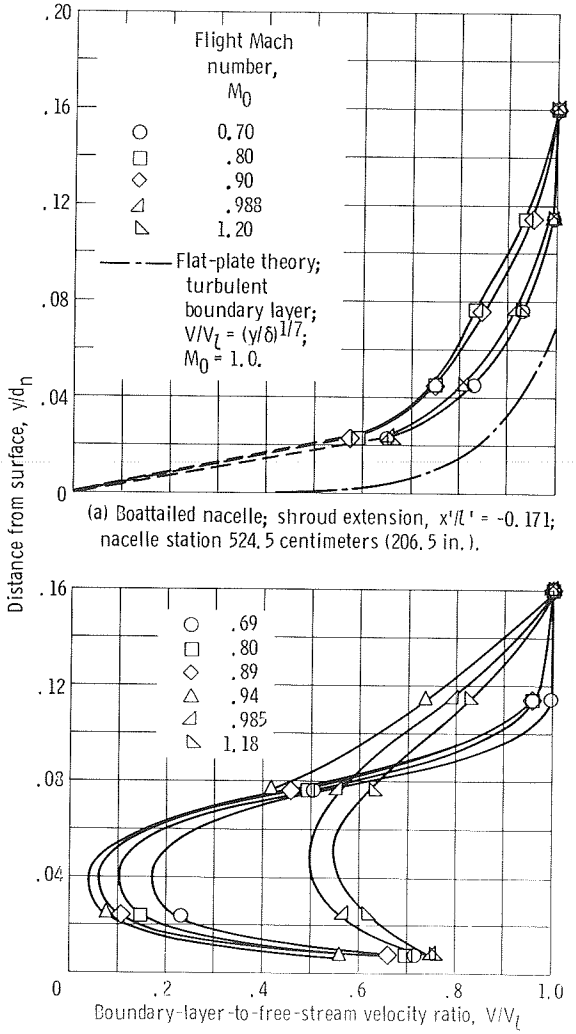

(a) Boattailed nacelle; shroud extension, $x'/l' = -0.171$; nacelle station 524.5 centimeters (206.5 in.).

(b) Tapered nacelle; shroud extension, $x/l = -0.08$; nacelle station 523.2 centimeters (206.0 in.).

Figure 33. - Effect of Mach number on boundary-layer velocity profile. Meridian angle, 180°; corrected secondary weight flow, $\omega\sqrt{\tau} = 0.03$.

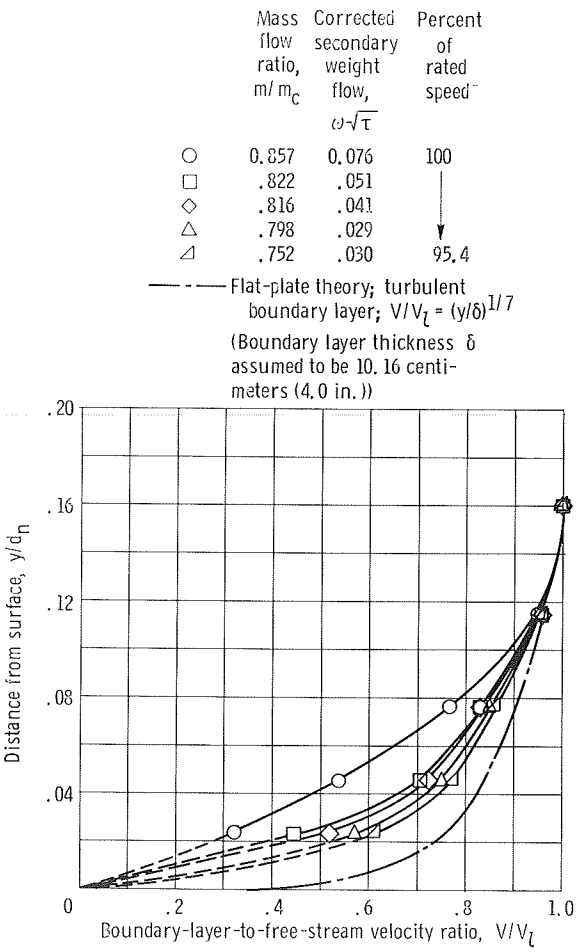

Figure 34. - Effect of inlet spillage on boundary-layer velocity profile. Meridian angle, 180°; nacelle station 524.5 centimeters (206.5 in.); flight Mach number, $M_0 = 0.9$. Boattailed nacelle; shroud extension, $x'/l' = -0.171$.

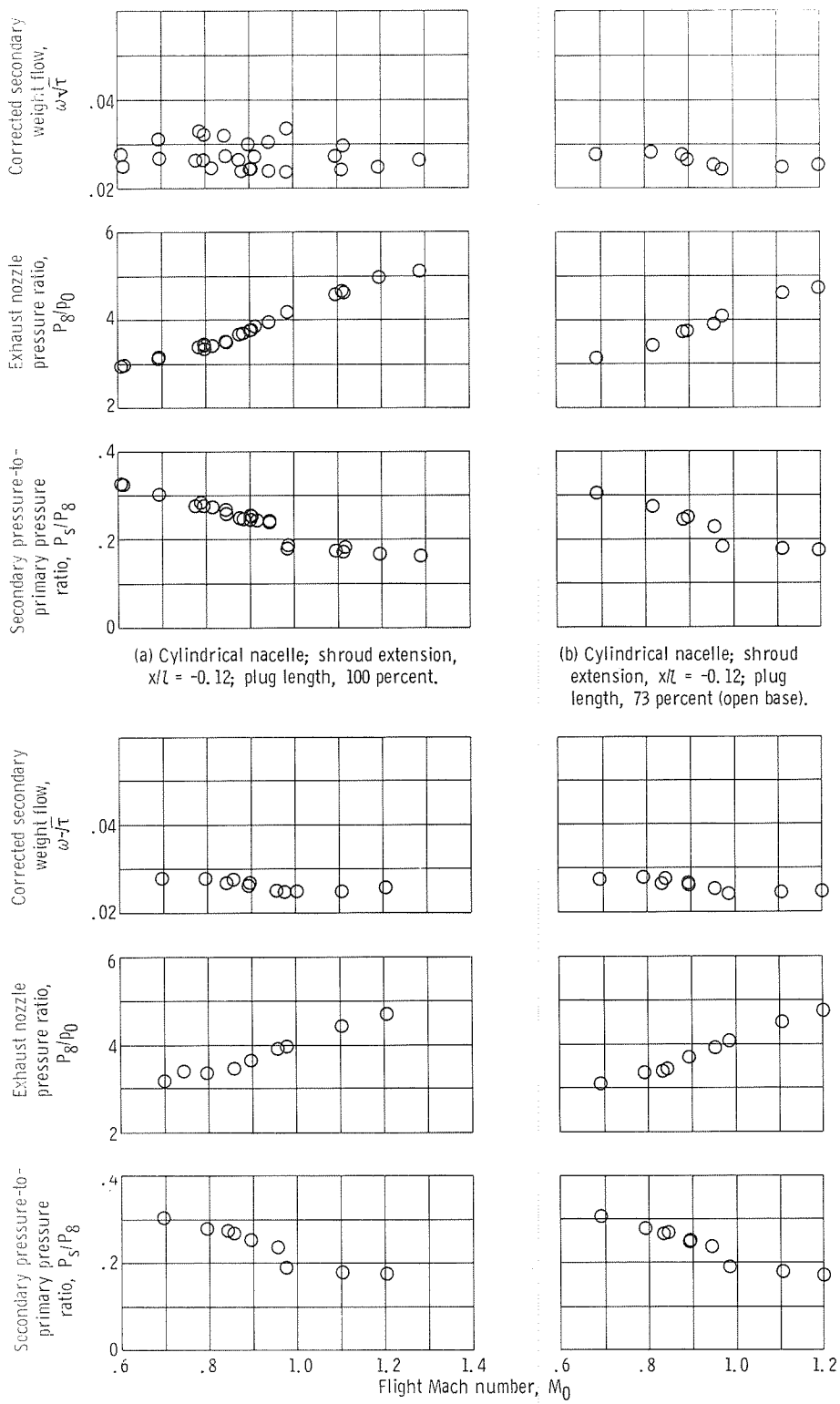

(a) Cylindrical nacelle; shroud extension, x/ℓ = -0.12; plug length, 100 percent.

(b) Cylindrical nacelle; shroud extension, x/ℓ = -0.12; plug length, 73 percent (open base).

(c) Cylindrical nacelle; shroud extension, x/ℓ = -0.12; plug length, 48 percent (open base).

(d) Cylindrical nacelle; shroud extension, x/ℓ = -0.12; plug length, 50 percent (closed base).

Figure 35. - Primary and secondary pressure conditions. Military power.

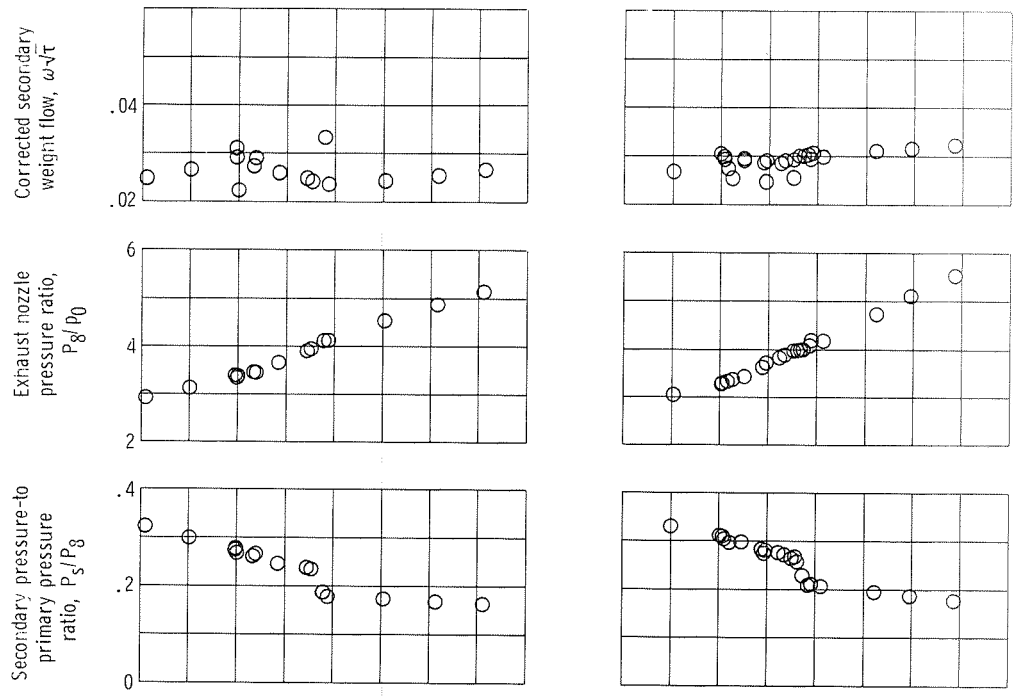

(e) Cylindrical nacelle; shroud extension, $x/\ell = -0.08$; plug length, 100 percent.

(f) Boattailed nacelle; shroud extension, $x'/\ell' = -0.171$; plug length, 100 percent.

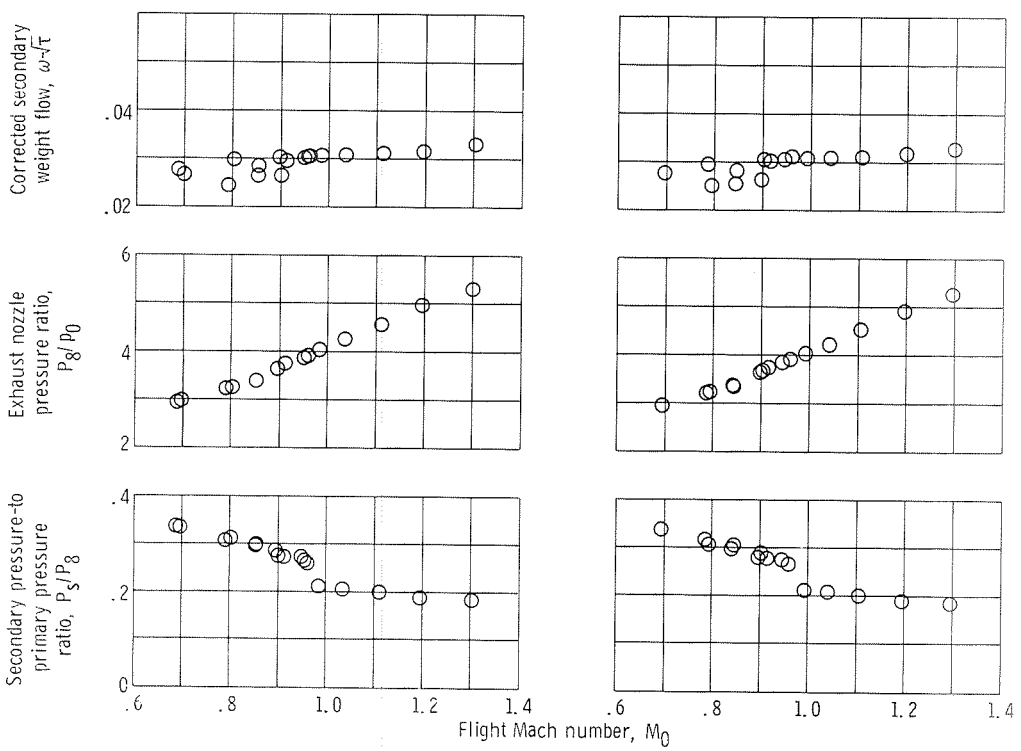

(g) Boattailed nacelle; shroud extension, $x'/\ell' = -0.171$; plug length, 67 percent (closed base).

(h) Boattailed nacelle; shroud extension, $x'/\ell' = -0.171$; plug length, 64 percent (open base).

Figure 35. - Continued.

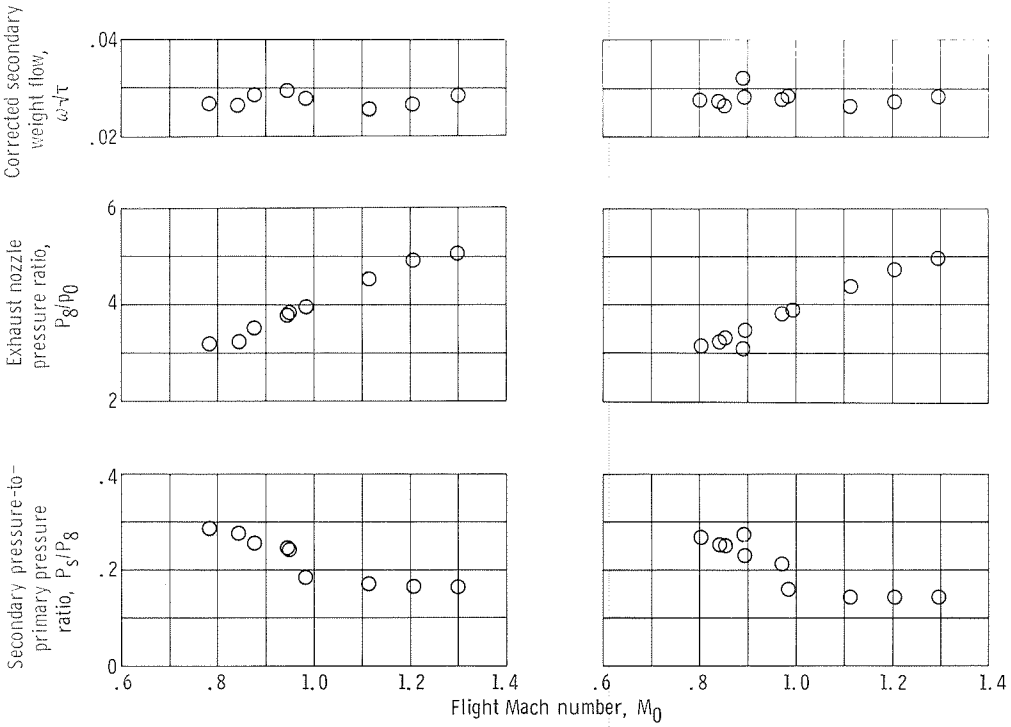

(i) Boattailed nacelle; shroud extension, $x'/l' = 0.005$; plug length, 100 percent.

(j) Boattailed nacelle; shroud extension, $x'/l' = 0.177$; plug length, 100 percent.

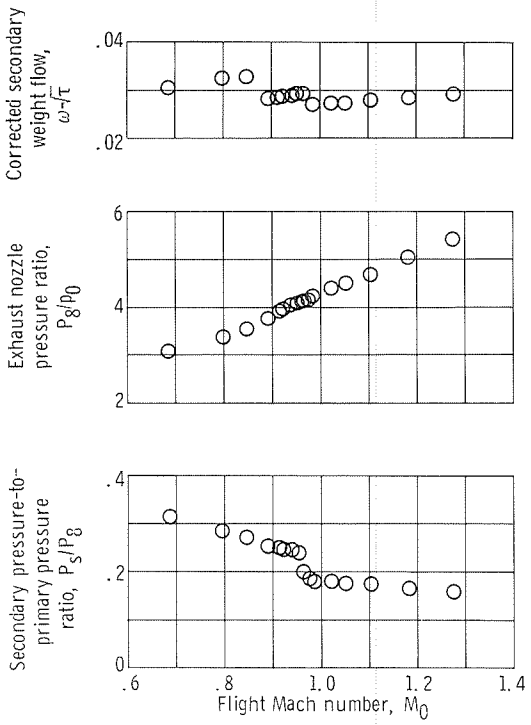

(k) Tapered nacelle; shroud extension, $x/l = -0.08$; plug length, 100 percent.

Figure 35. - Concluded.

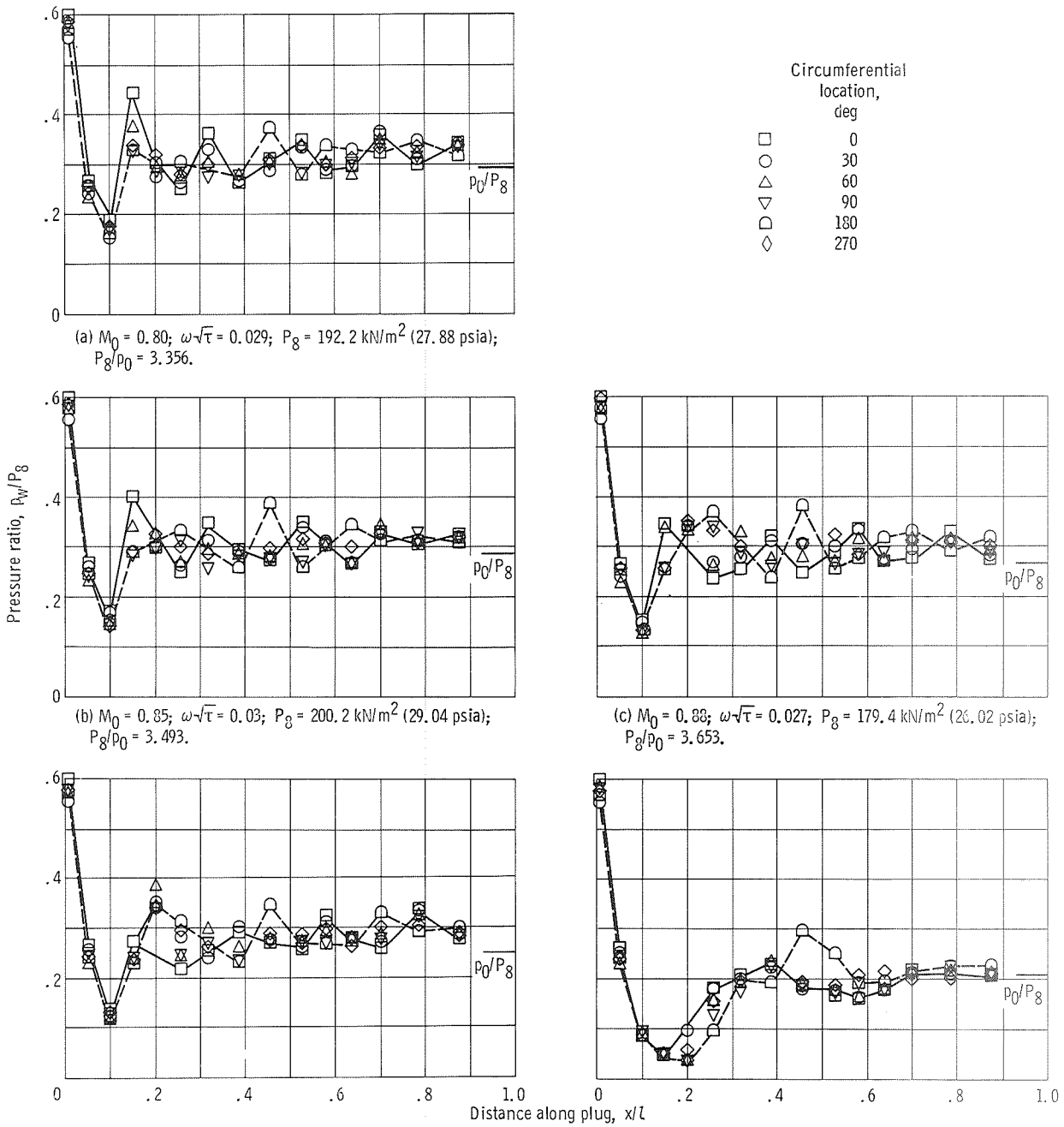

(a) $M_0 = 0.80$; $\omega\sqrt{\theta} = 0.029$; $P_8 = 192.2$ kN/m^2 (27.88 psia); $P_8/p_0 = 3.356$.

(b) $M_0 = 0.85$; $\omega\sqrt{\theta} = 0.03$; $P_8 = 200.2$ kN/m^2 (29.04 psia); $P_8/p_0 = 3.493$.

(c) $M_0 = 0.88$; $\omega\sqrt{\theta} = 0.027$; $P_8 = 179.4$ kN/m^2 (26.02 psia); $P_8/p_0 = 3.653$.

(d) $M_0 = 0.95$; $\omega\sqrt{\theta} = 0.03$; $P_8 = 163.4$ kN/m^2 (23.70 psia); $P_8/p_0 = 3.928$.

(e) $M_0 = 1.19$; $\omega\sqrt{\theta} = 0.025$; $P_8 = 188.2$ kN/m^2 (27.29 psia); $P_8/p_0 = 4.972$.

Figure 36. - Pressure variation along plug surface of cylindrical nacelle ($x/l = -0.12$) for various flight Mach numbers M_0, corrected secondary weight flows $\omega\sqrt{\theta}$, primary nozzle total pressures P_8, and nozzle pressure ratios P_8/p_0. Military power; plug length, 100 percent.

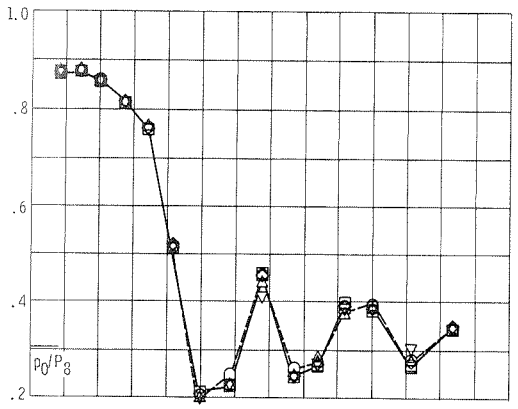

Circumfrential location, deg

□	0
○	30
△	60
▽	90
⊓	180
◇	270

(a) M_0 = 0.80; $\omega\sqrt{\tau}$ = 0.029; P_8 = 192.2 kN/m^2 (27.87 psia); P_8/p_0 = 3.323.

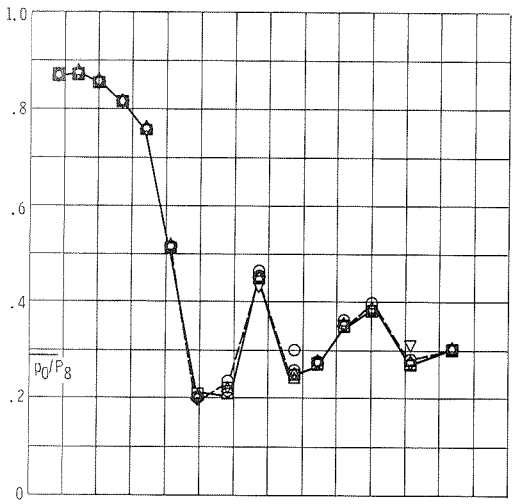

Pressure ratio, P_w/P_8

(b) M_0 = 0.85; $\omega\sqrt{\tau}$ = 0.03; P_8 = 197.5 kN/m^2 (28.64 psia); P_8/p_0 = 3.416.

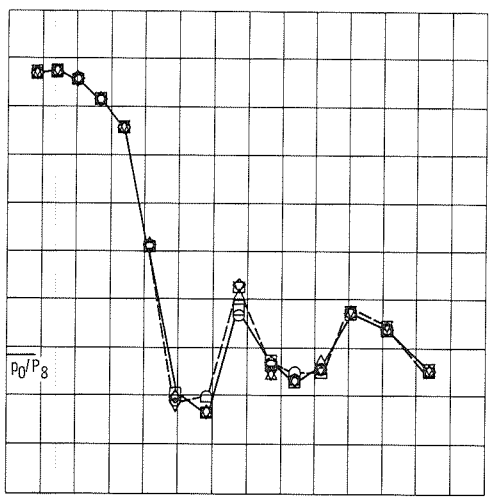

(c) M_0 = 0.90; $\omega\sqrt{\tau}$ = 0.029; P_8 = 174.7 kN/m^2 (25.34 psia); P_8/p_0 = 3.691.

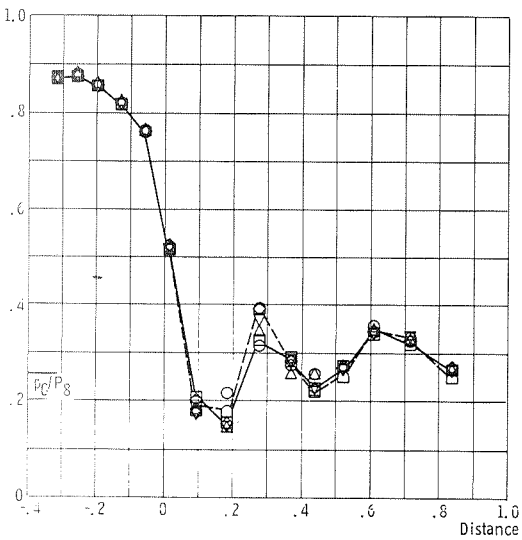

(d) M_0 = 0.95; $\omega\sqrt{\tau}$ = 0.029; P_8 = 162.6 kN/m^2 (23.59 psia); P_8/p_0 = 3.934.

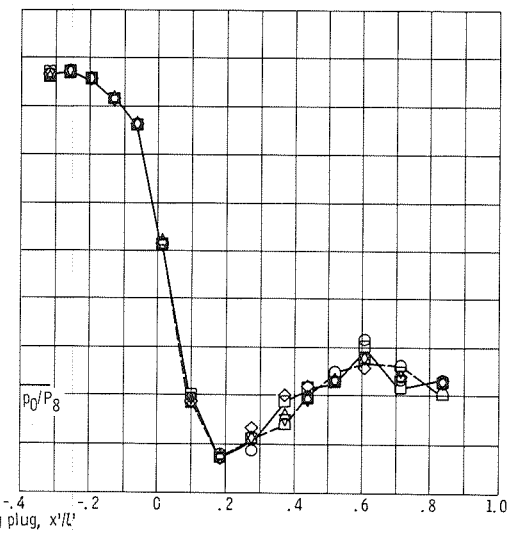

Distance along plug, x'/l'

(e) M_0 = 1.12; $\omega\sqrt{\tau}$ = 0.03; P_8 = 176.5 kN/m^2 (25.60 psia); P_8/p_0 = 4.712.

Figure 37. - Pressure variation along plug surface of boattailed nacelle (x'/l' = -0.171) for various flight Mach numbers M_0, corrected secondary weight flows $\omega\sqrt{\tau}$, primary nozzle total pressures P_8, and nozzle pressure ratios P_8/p_0. Military power; plug length, 100 percent.

NASA-Langley, 1971 — 1 E-5546

NATIONAL AERONAUTICS AND SPACE ADMINISTRATION
WASHINGTON, D. C. 20546

OFFICIAL BUSINESS
PENALTY FOR PRIVATE USE $300

FIRST CLASS MAIL

POSTAGE AND FEES PAID
NATIONAL AERONAUTICS AND
SPACE ADMINISTRATION

POSTMASTER: If Undeliverable (Section 158 Postal Manual) Do Not Return

"The aeronautical and space activities of the United States shall be conducted so as to contribute . . . to the expansion of human knowledge of phenomena in the atmosphere and space. The Administration shall provide for the widest practicable and appropriate dissemination of information concerning its activities and the results thereof."

—NATIONAL AERONAUTICS AND SPACE ACT OF 1958

NASA SCIENTIFIC AND TECHNICAL PUBLICATIONS

TECHNICAL REPORTS: Scientific and technical information considered important, complete, and a lasting contribution to existing knowledge.

TECHNICAL NOTES: Information less broad in scope but nevertheless of importance as a contribution to existing knowledge.

TECHNICAL MEMORANDUMS: Information receiving limited distribution because of preliminary data, security classification, or other reasons.

CONTRACTOR REPORTS: Scientific and technical information generated under a NASA contract or grant and considered an important contribution to existing knowledge.

TECHNICAL TRANSLATIONS: Information published in a foreign language considered to merit NASA distribution in English.

SPECIAL PUBLICATIONS: Information derived from or of value to NASA activities. Publications include conference proceedings, monographs, data compilations, handbooks, sourcebooks, and special bibliographies.

TECHNOLOGY UTILIZATION PUBLICATIONS: Information on technology used by NASA that may be of particular interest in commercial and other non-aerospace applications. Publications include Tech Briefs, Technology Utilization Reports and Technology Surveys.

Details on the availability of these publications may be obtained from:

SCIENTIFIC AND TECHNICAL INFORMATION OFFICE

NATIONAL AERONAUTICS AND SPACE ADMINISTRATION

Washington, D.C. 20546